

Applying the Material Point Method to Identify Key Factors Controlling Runout of the Cadia Tailings Dam Failure of 2018

Ian W. Pierce

Thesis submitted to the Faculty of the
Virginia Polytechnic Institute and State University
in partial fulfillment of the requirements for the degree of

Master of Science
in
Civil Engineering

Alba Yerro-Colom, Chair

Thomas L. Brandon

Russell A. Green

June 21, 2021

Blacksburg, Virginia

Keywords: Tailings Dam, Numerical Modeling, Material Point Method, Cadia, Liquefaction

Copyright 2021, Ian W. Pierce

Applying the Material Point Method to Identify Key Factors Controlling Runout of the Cadia Tailings Dam Failure of 2018

Ian W. Pierce

ABSTRACT

This thesis examines the 2018 failure of the Northern Tailings Storage Facility at Cadia Valley Operations, located in New South Wales, Australia. First, the importance of examining and understanding failure mechanisms and post failure kinematics is described. Within which we understand that in the current state of affairs it is exceedingly difficult, or nigh impossible to perform without the use of large strain analyses, which have yet to permeate into the industry to a significant degree. Second, the initial construction and state of the dam just prior to failure is defined, with the materials and their properties laid out and discussed in depth as well as our means of modeling their behavior. Third, we validate and discuss our results of the base model of the dam based on key topographic features from initial and post-failure field measurements. After validation, we examine the influences of each of the different materials on the runout, comparing final topographies of different simulations with the actual final topography observed. This study was a valuable method of validating the Material Point Method as a means of modeling large deformations, as well as demonstrating its powerful applications towards catastrophic disaster prevention. The study validates and provides a greater understanding of the event of the Cadia Tailings Storage Facility Failure, and presents a framework of steps to perform similar examination on future tailings dams as a means of providing risk management in the event of failure.

Applying the Material Point Method to Identify Key Factors Controlling Runout of the Cadia Tailings Dam Failure of 2018

Ian W. Pierce

GENERAL AUDIENCE ABSTRACT

Tailings dams are structures integral to the life cycle of mining and mineral processing. After mining and the processing of mined materials, the leftover material, known as "tailings" are pumped and stored behind these structures, usually indefinitely. These structures are unique because they are usually expanded as additional storage space for these materials is required. Over the past several decades, the rate at which catastrophic or serious tailings dam failures occur out of failures has been on the rise. Because of this, it becomes necessary to better understand the failure and post-failure movements of the dam. This thesis presents one such failure, the Cadia Tailings Dam Failure of 2018, which is located in New South Wales, Australia. It applies the Material Point Method, a numerical method which allows for large-strain deformations, to examine the post-failure mechanism and interpret various influences by the different materials on the final runout. Because of this, the paper provides insights on the importance of understanding large strain analyses, discussing and presenting the incidents of the failure. The model used for reference is validated using topographic and field data taken after the failure, allowing for a comparison with future models which vary the geometry and material characteristics of the event. A procedural plan is proposed to apply to future analyses, allowing for the analysis to be applied to other events and tailings dam structures, for further insight on influences of variability and material properties on post-failure topography and geometry.

Acknowledgments

First and foremost, I would like to thank my advisor, Prof. Alba Yerro-Colom. Her knowledge, encouragement, and adaptability as we navigated our work during the pandemic of COVID-19 were invaluable, and my gratitude for it all is ineffable, as I would certainly not have made it this far but for her taking me under her wing in my pursuit of knowledge, much of which is distilled here in this thesis.

I would like to thank Prof. Thomas Brandon and Prof. Russell Green for serving on my thesis review committee, and for pushing me in my coursework during the pursuit of my masters degree. Both of them served to inspire and push me to be the best I could be.

I would be remiss to not also mention Prof. Matthew Mauldon, Prof. Adian Rodriguez-Marek, Prof. George Filz, Prof. Sherif Abdelaziz, and Prof. Joseph Dove for their teaching and mentorship during my graduate coursework and graduate assistanceships. In particular, I should thank Professors Mauldon and Dove, as well as Julie Paprocki for instilling and sharing with me a love of geotechnical engineering in my undergraduate years.

Outside of the Geotechnical Engineering program, I would like to extend my gratitude to Prof. Christopher Galitz and Prof. Paolo Scardina for encouraging me to pursue my graduate degree, particularly to Prof. Galitz for his continued mentorship during my first semester.

Within my research group, I would like to thank Abdelrahman Alsardi, Luis Zambrano-Cruzatti, and Kayleigh Yost. Their feedback, assistance, and friendship were truly a boon, and without them I would not be where I am on this day.

At Georgia Tech, I would like to thank Dr. Jorge Macedo and his student Renzo Cornejo for serving in a consultational capacity as we evaluated material modeling and behaviors.

I would like to thank my family and friends, particularly my parents Chris and Kathy, two sisters, Courtney and Corabeth, and my friends Michael, Ryan, and Rebekah for their support and understanding as I navigated the waters leading to the creation of this paper.

Contents

- List of Figures ix

- List of Tables xii

- List of Abbreviations xiii

- 1 Introduction 1**
 - 1.1 Motivation 1
 - 1.2 Research Objectives 3
 - 1.3 Organization 4

- 2 Background 5**
 - 2.1 Construction 5
 - 2.2 Failure 9
 - 2.3 Post-failure investigation 10
 - 2.3.1 Testing & Materials 11
 - 2.3.2 Limit Equilibrium Analysis 14
 - 2.3.3 Small-Deformation Analysis 14
 - 2.3.4 Runout Data 18

2.4	Causes of failure	18
3	Material Point Method	20
3.1	MPM Method	20
3.2	Reasons for Selection	21
3.3	Applications	22
4	MPM Model	24
4.1	Geometry	24
4.2	Materials	26
4.2.1	Dam	26
4.2.2	Tailings	27
4.2.3	Foundation	29
4.3	Calculation Phases	32
5	Results	35
5.1	Comparison of the reference model with topographic and field data	35
5.2	Post-failure mechanism and kinematic behavior of the Cadia dam failure	37
5.3	Influence of the tailings	39
5.3.1	Liquefaction Extent	39
5.3.2	Rate of Liquefaction Triggering	40
5.3.3	Liquefied tailings Strength	42

5.4	Influence of the brittle foundation	44
5.5	Influence of excavation and buttress (Stage 10)	47
6	Conclusions	49
6.1	Safety & Importance	49
6.2	Material Influence	50
6.3	Future Work	51
6.4	Closing Thoughts	52
	Bibliography	53

List of Figures

2.1	Stage 1 of Construction [1]	6
2.2	Stages 2A and 2B of Construction [1]	7
2.3	Stage 3 of Construction [1]	7
2.4	Stages 4-9 of Construction [1]	8
2.5	Stage 10 of Construction [1]	8
2.6	Satellite Photo of Failure [1]	9
2.7	Topography just after failure in March 10, 2018 [1]. Units in meters	10
2.8	Final Topography (March 14, 2018) [1]. Units in meters	10
2.9	LEA Model modified from ITRB [1] to Model Potential Failure Surfaces	15
2.10	Numerical Conclusions modified from ITRB [1] Using FLAC: Visualization of Progressive Softening of Foundation Under Construction. Units in meters.	16
2.11	Numerical Conclusions Modified from ITRB [1] Using FLAC: Instability Ratio of Tailings at Final Two Stages of Construction	17
2.12	Simplified Boring Log of CE433 From Post-Failure Investigation	18
3.1	Graphical Representation of MPM Computation Cycle (from Yerro, 2015) [2]	21
4.1	Reference Model Geometry (units in meters)	25
4.2	Computational Mesh of Model (units in meters)	26

4.3	Calibration Plot of FRVA	32
4.4	Stress Initialization: Total Vertical Stress	33
4.5	Stress Initialization: Pore Water Pressures	33
5.1	Final Runout: Reference Model (units in meters) [Model 1]	36
5.2	Digitized Borehole Comparison	37
5.3	Failure plane progression through deviatoric strain at different times after the failure triggering (distance in meters)	38
5.4	Reference Model with Velocity Plotted at Various Times (distance in meters)	39
5.5	Final Runout: No Liquefaction (units in meters) [Model 2]	40
5.6	Final Runout: First Zone Liquefies (units in meters) [Model 3]	41
5.7	Final Runout: Fourth Zone of Liquefaction (units in meters) [Model 4]	41
5.8	Final Runout: Reduced Rate of Liquefaction, 10 seconds Between Liquefied Zones (units in meters) [Model 5]	42
5.9	Final Runout: All Zones Liquefied at Failure Initiation (units in meters) [Model 6]	43
5.10	Final Runout: Low Liquefied Tailing Strength (3 kPa) (units in meters) [Model 7]	43
5.11	Final Runout: High Liquefied Tailing Strength (30kPa) (units in meters) [Model 8]	44
5.12	Final Runout: Varied Liquefied Tailing Strength with Depth (units in meters) [Model 9]	45

5.13	Final Runout: No Strain Softening in FRV (units in meters) [Model 10]	45
5.14	Failure progression through deviatoric strain at different times of failure with no strain softening	46
5.15	Final Runout: Strain Softening Included in FRVB (units in meters) [Model 11]	46
5.16	Final Runout: Reduced Residual Strength in FRVA (units in meters) [Model 12]	47
5.17	Final Runout: No Buttress Constructed, No Excavation & Tailings Liquefy (units in meters) [Model 13]	48

List of Tables

4.1	Rockfill Characteristics	27
4.2	Tailings Characteristics	28
4.3	Foundation Characteristics	32
6.1	Summary of Simulation Runout Results	50

List of Abbreviations

CPT	Cone Penetrometer Test
CVO	Cadia Valley Operations
DSS	Direct Simple Shear
FDM	Finite Difference Method
FEA	Finite Element Analysis
FEM	Finite Element Method
FFP	Free Fall Penetrometer
FRV	Forest Reef Volcanics
FRVA	Forest Reef Volcanics Unit A
FRVB	Forest Reef Volcanics Unit B
FS	Factor of Safety
ICU	Isotropically Consolidated Undrained
ITRB	Independent Tailings Review Board
LEA	Limit Equilibrium Analysis
LEM	Limit Equilibrium Method
MPM	The Material Point Method

Chapter 1

Introduction

1.1 Motivation

The safety and risk associated with tailings dam failures has been on the rise in recent years and is a topic of international debate. Over the past three decades, the number of serious to disastrous tailings dam failures has increased from 14 to 31% [3]. A rate increase of more than double is concerning, because catastrophic consequences of a tailings dam failure often include not only large impacts on the environment, but also the loss of human life. This danger is highlighted most recently by the 2019 Brumadinho Dam failure in Brazil [4], where over 250 people died as a result of the failure, and by the 2015 Fundao Dam failure, where approximately 40 million cubic meters of toxic sludge were spilled into downstream communities.

In August of 2020, a new international standard on tailings management was created by the United Nations [5]. This standard calls for zero harm to people or the environment in the event of failure. The clear risk and hazard posed as the result of these potential tailings dam failures (already in place or in future constructed facilities) means that it is important to be able to understand and predict the risks and hazards associated with such catastrophic events. The importance and complexity of the interactions between the unique materials, topography, climate, and additional situations associated with the different failures cannot be overstressed. Therefore, there is a need to better understand the consequences of failure,

as well as the influence of the pre-failure conditions on the extent and rate of runout, and danger to downstream communities.

The report on the Mount Polley Failure of 2014 [6] describes just how crucial this can be: “[Tailings Dams] are unforgiving systems, in terms of the number of things that have to go right. Their reliability is contingent on consistently flawless execution in planning, in subsurface investigation, in analysis and design, in construction quality, in operational diligence, in monitoring, in regulatory actions, and in risk management at every level. All of these activities are subject to human error.” With the risk of human error always present in any of these crucial steps, the use of numerical modeling is of great importance to understand the influence of variability of site characteristics in new and pre-existing dams. In particular, the use of the Material Point Method (MPM) proves to be valuable, due to its large strain deformation simulation capabilities, which can be demonstrated to help offset or even negate catastrophic failures like the Brumadinho failure.

The simulation of post-failure runout requires the use of numerical techniques capable of dealing with large deformations of the ground, complex multi-material geometries, history-dependent materials, and hydro-mechanical coupling. Numerically, this is extremely challenging. Traditionally, for the design of tailings dam structures and predict their associated risks, designers use simplified numerical tools used to calculate water dam-breaks that are incapable of dealing with such complexities. However, this is insufficient for such things as tailings dams, where the tailings do not necessarily liquefy [7]. More recently in geotechnical engineering, several advanced numerical frameworks, including MPM, are emerging and being developed to address these challenges. These are currently being validated in a number of different applications.

This research concentrates on the simulation of the Cadia tailing dam failure using MPM, and serves as one such validation of MPM. In March of 2018, the Northern Tailings Storage

Facility (NTSF) of the Cadia Valley Operations (CVO) gold and copper mining facility in New South Wales failed during renovation and expansion of the dam which were intended to allow for increased capacity. Due to the observation of tension cracks during the workday and an appropriate response, the site was evacuated before failure occurred. Approximately 1.3 million cubic meters of material were released into the downstream storage, with a runout of approximately 170 meters. This research presents the first runout analysis of this event. This is relevant because contributes to the validation of MPM and builds up a certain level of confidence on this numerical method for the application on the study and design of tailings dams and retaining facilities.

1.2 Research Objectives

The main aims of the research conducted and given in this thesis are:

- Review previous analysis of the 2018 Cadia Tailings Dam Failure provided by the Independent Tailings Review Board (ITRB). This includes construction history, field and laboratory data, pre and post-failure topography, stability analysis.
- Create a numerical model using the Material Point Method (MPM) which can successfully simulate the post failure kinematics and final runout of the event.
- Use the created numerical model to examine the influence of different material properties and geometry of the dam on final runout.
- Demonstrate a methodology which can be replicated for future dams using the MPM as a means of examining the scale of runout and influence of material and site properties.

1.3 Organization

This thesis is laid out in such a way as to provide the reader with sufficient background information as to be able to understand the process taken to understand and model the 2018 Cadia Dam failure. Chapter 2 provides relevant background information on the history of the failure, such as construction information and designs from prior to failure, initial response after the failure, field and laboratory data gathered, and subsequent slope stability analysis. It also provides the metrics by which our own work is later verified and checked. Chapter 3 presents MPM as the means we are modeling the failure and post-failure runout, briefly introduces the basis of the method and the computational cycle, and discusses some of the additional applications MPM has been used for. Chapter 4 introduces the numerical MPM model developed in this research. It is broken down into several subsections: First, the geometry and makeup of the model is presented. Next, the calculation phases are defined, describing the process by which we simulate the failure event. Finally, the material properties considered for the different materials are discussed, and reference to laboratory tests supporting the selected properties is provided. Chapter 5 presents the results of the MPM model. Particular attention is given to the comparison with the available post-failure reference data. After the validation, the results from a parametric analysis are presented to examine the impact of material properties and geometry on the final runout. Finally, Chapter 6 presents the conclusions of the research and discusses potential next steps to better refine the results for 2018 Cadia Dam failure or for future analyses of other dam failures.

Chapter 2

Background

This chapter is broken down into four main sections. The first section describes the construction of the Cadia tailings dam, which occurred across multiple stages of construction over 20 years. The second section describes the failure event. The third section presents the post-failure response, which prompted the creation of an independent review board which performed field and laboratory tests as well as limit equilibrium and small deformation analyses to examine probable contributions to the failure. This includes the description of the materials. The final section describes the data provided in the third section, and presents it as a way to validate the MPM model presented in Chapters 4 and 5.

2.1 Construction

The dam is the result of 10 different stages of construction between 1998-2018, with the first phases of the dam making use of downstream expansion, before transitioning into an upstream expansion technique. Stage 10 was under construction at the time of the failure event, and had not yet been completed. Tailings were put in place using a rail mounted pumping system to ensure the deposition remains subaerial. Multiple spigots from a header pipeline run along the embankment crest, with tailings falling to a decant pool at the upstream end of the storage area. The staged construction illustrations included below are pulled from the ITRB Report [1].

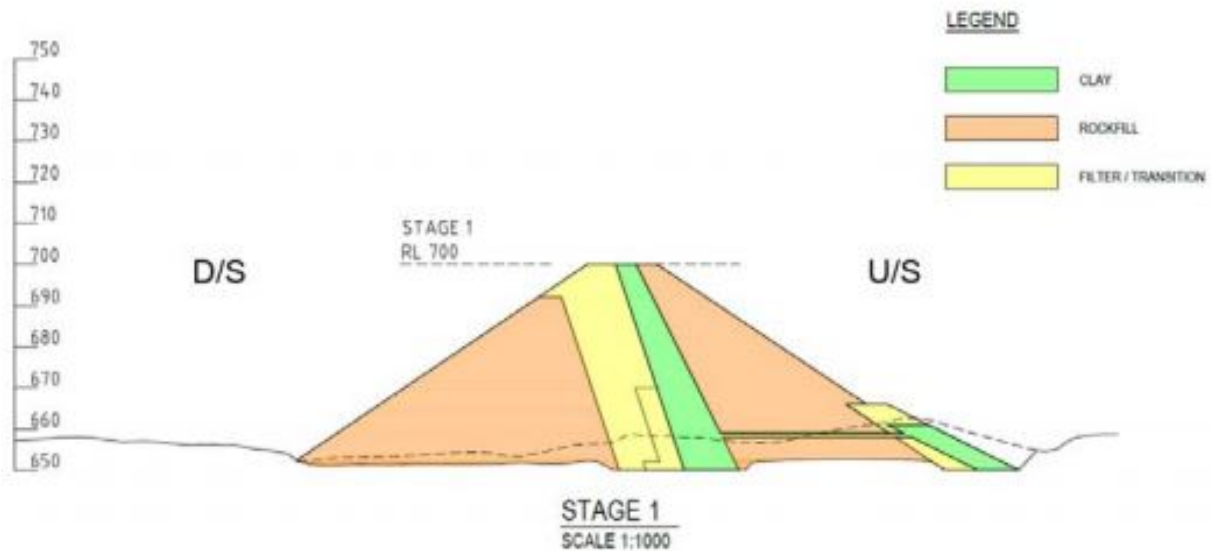


Figure 2.1: Stage 1 of Construction [1]

Stage 1 is the initial constructed dam, with a maximum height of 50 meters, and the cross section of this stage is shown in Figure 2.1. The original design plan for the dam was to construct the dam with future phases moving downstream, as is the case with Stages 2A & 2B shown in Figure 2.2. These two substages are each 3.5 meters in height. In Stage 3, the dam expansion began to transition into an upstream type of construction, with a 4.5 meter raise to the dam, shown in Figure 2.3. Stages 4 through 9 are individual upstream raises to the dam, with heights ranging from 3 to 6 meters, shown in Figure 2.4.

Stage 10 of the dam was under construction when the dam failed in March of 2018. This stage consisted of a 3 meter raise to the dam. Based upon CPT tests taken in 2017, the designers determined that the factor of safety of the dam was too low, and as such recommended the construction of two buttresses to provide additional stability to the dam. These buttresses are shown in the cross section, Figure 2.5, with buttress stage 2 of the dam not yet constructed in the location of failure. Prior to starting construction of buttress stage 2, the area below it was excavated to remove loose tailings which had pooled in that location.

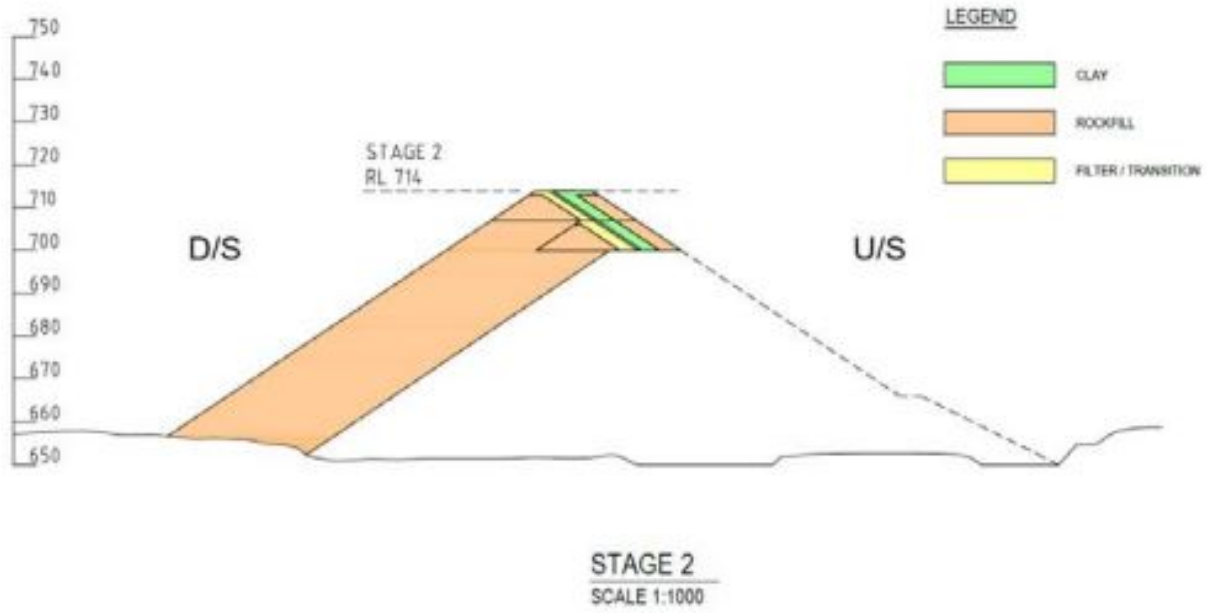


Figure 2.2: Stages 2A and 2B of Construction [1]

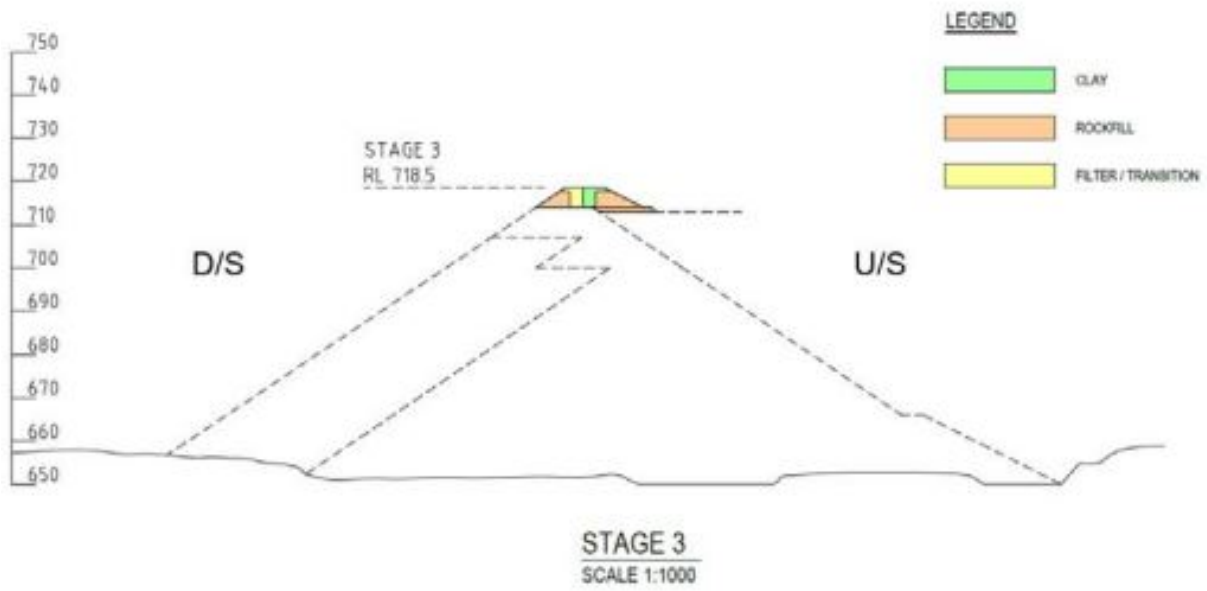


Figure 2.3: Stage 3 of Construction [1]

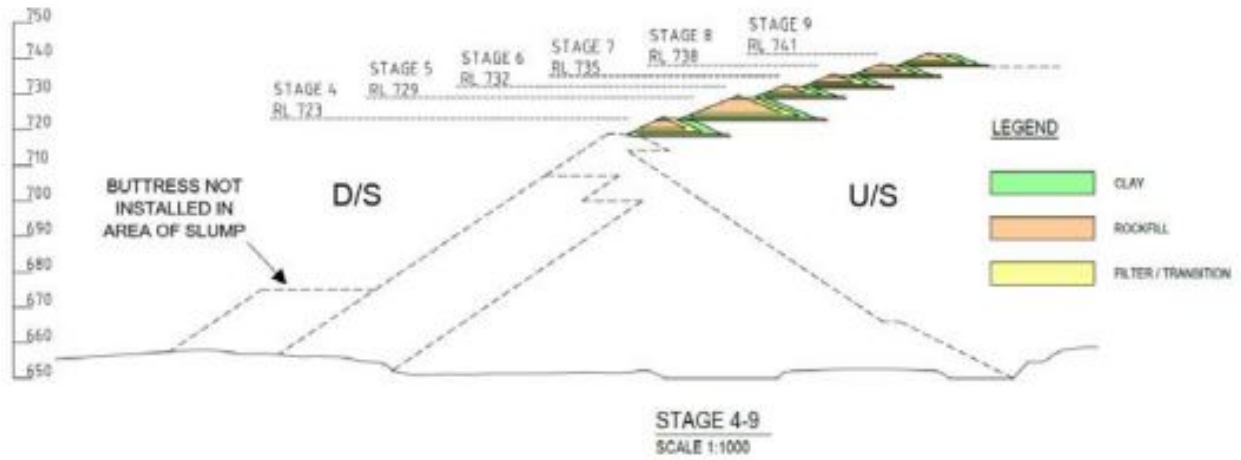


Figure 2.4: Stages 4-9 of Construction [1]

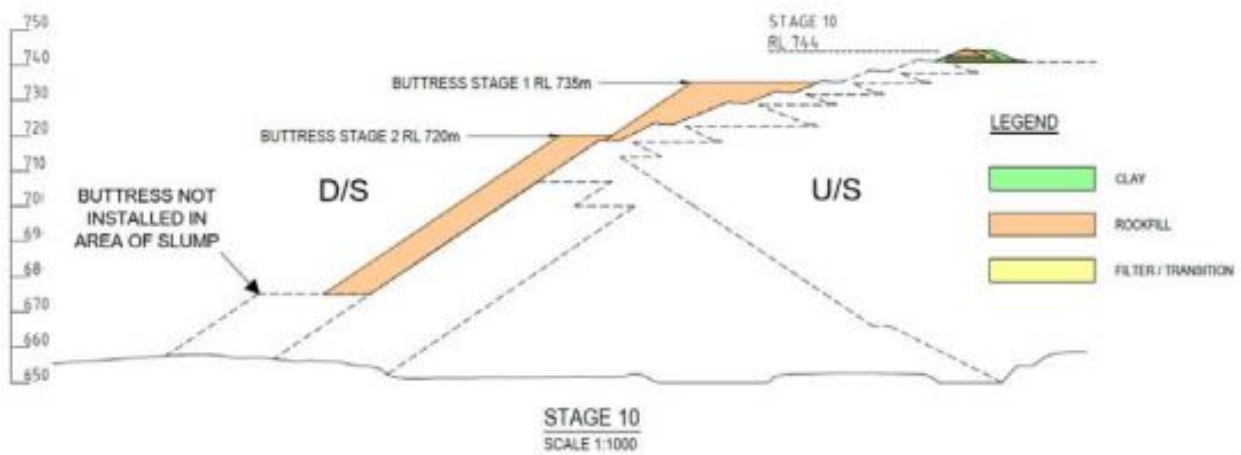


Figure 2.5: Stage 10 of Construction [1]

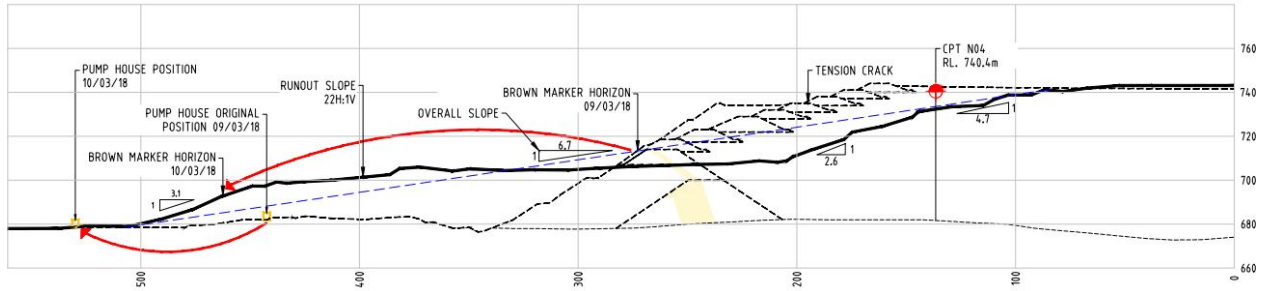


Figure 2.7: Topography just after failure in March 10, 2018 [1]. Units in meters

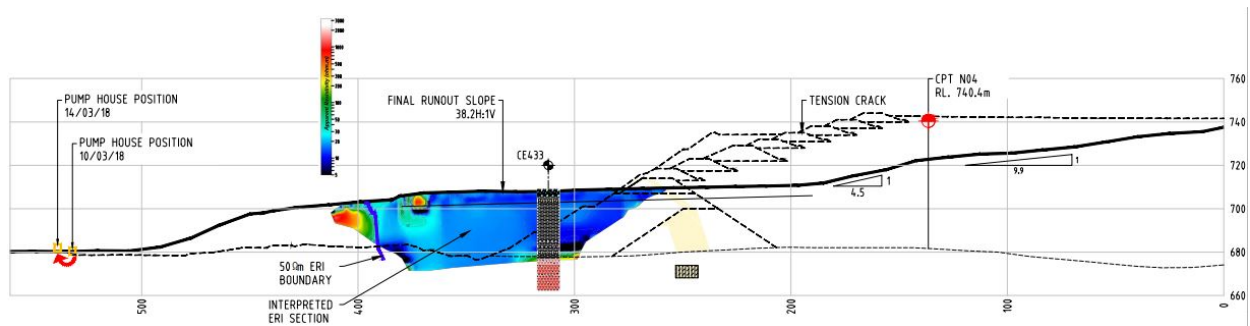


Figure 2.8: Final Topography (March 14, 2018) [1]. Units in meters

2.3 Post-failure investigation

After the failure, the owners engaged with Ashurst, Australia to put together the ITRB, which would review the failure to determine the causes of the failure and its propagation. The committee performed field investigations coupled with laboratory tests, which included soil classification, direct simple shear (DSS) tests and triaxial tests to evaluate properties of the materials involved. These results were applied to Limit Equilibrium Analysis (LEA) as well as small-deformation numerical modeling using the software FLAC.

Initial response to the failure included the collection of topographical information which is shown in figures 2.7 & 2.8. Within the two days after the initial failure, the tailings again experienced local instabilities as the time allowed for the drainage to release suctional pore water pressures from the tailings which had been generated in the initial failure.

In addition to topography data, borings were taken along with samples for laboratory testing. Non-invasive testing was used to provide an approximate idea on the extent and distribution of the tailings below the surface of the dam. A cross section of with some of these data is shown in Figure 2.8.

After initial field investigations, many laboratory tests were conducted to determine the properties of the materials involved in the failure. These laboratory tests included DSS tests, triaxial tests, taking Atterberg limits and soil identification, and CPT.

2.3.1 Testing & Materials

A description of the different materials in the site is included below. Three main zones are distinguished: tailings, foundation, and dam.

Dam

The dam is composed of three different zones: the rockfill, the transition zone, and the clay core (indicated in orange, yellow, and green respectively) in Figures 2.1-2.5.

Because of the cost prohibition involved with testing the rockfill, the strength and stiffness of this material was obtained in design through literature. ITRB used an approximation of the strength based upon confining pressure which ranged in drained friction angles of 40-50°, using information from Indraratna et al. (1993) [8]. This was later simplified to 40° in their analyses. Stiffness was determined to be approximately 65 MPa, based upon review in Fell Hunter (2002) [9] and Hunter (2003) [10]. The density of the material was estimated to range from 1900-2000 kg/m³.

Transition zone materials were intended to provide filtration properties to the dam in early

stages of construction. Limited data on this material is available, as it was specified in construction primarily based upon gradation requirements, which specified it to comprise of sand-sized material. In the ITRB Report [1], they consider a drained friction angle of 42° to describe the shear strength of the transition zone.

Finally, clay core testing was performed through re-compacted ICU triaxial tests, with resulting strengths ranging from approximately $17.5\text{-}22.1^\circ$, with a cohesion of 16 kPa.

Tailings

The characterization of the tailings is complex. Their contractive behavior and strain softening when loaded in undrained conditions, coupled with their variable properties in relation to confinement result in a unique behavior which is difficult to characterize and model. Extensive laboratory and field testing was performed to determine the tailing's properties. This included field Cone Penetrometer Testing (CPT), Cyclic DSS tests, stress-path triaxial testing, as well as other tests to determine minerology, grain shape, Atterberg limits, and specific gravity.

The tailings are composed of silty sand and sandy silt materials, which are susceptible to liquefaction. Results from triaxial tests indicated an approximate peak drained strength of 34° . CPTu data was used to create and check the calibration of a NORSAND model used in small-deformation analysis. The in-situ state parameter (ψ) as well as the tailings' brittleness (proportion of undrained strength lost on liquefaction) are estimated based on CPTu data postprocessing. The state parameter is predicted to be between 0.06 and 0.08, which confirms the contractive behavior of the material and the tendency to generate excess pore pressure when undrained loading. The brittleness results are also consistent with previous case histories of flow liquefaction reported in Robertson (2017) [11], indicating that

the tailings where highly susceptible to liquefaction. Drained and undrained triaxial tests were used to determine the ultimate critical state line (characterized by M_t , which is the stress ratio at critical state) as well as the instability locus (instability line) for different triaxial loading stress paths similar to the in-situ staged construction. The instability locus (characterized by η_{il}) is much affected by the state parameter, the drainage, and the loading conditions. In particular, it was observed that $M_f < \eta_{il}$ in undrained conditions, meaning that soil collapses (liquefaction) before reaching critical state when the stress state exceeds the soil's instability locus.

Finally, cyclic DSS tests were performed to provide information on the sensitivity of the tailings to liquefaction in the event of earthquakes. Seismic dilatometer tests were performed in an area near the failure to obtain the Young's Modulus, and was found to vary with depth from 20-144 MPa.

Foundation

The foundation is made up of five different materials as a result of volcanic activity and subsequent weathering. Of primary interest to the failure investigation was the Forest Reef Volcanic (FRV) material, due to its location directly below the dam structure in the area where the dam failed. The FRV is zoned into two units, Unit A (FRVA) and Unit B (FRVB). FRVA is the upper of the two units, and exhibits strain-softening tendencies. FRVB is underlain by stiff bedrock. The FRV varies in thickness significantly, between 8 and 20 meters.

Consolidation testing and DSS testing were the primary tests performed on all the foundation materials. Additionally, CIU triaxial stress path tests were performed on FRVA, as well as three Direct Shear tests and one Ring Shear test on remoulded samples. Because of the

limitations of a DSS test, it is impossible to achieve a true residual strength or Skempton's fully-softened state [12]. For clarity, it is understood that when referring to "softened" material in this thesis, it is not in a fully-softened or residual state, unless specified as such. The results of these tests showed a great deal of variability in the strength of the foundation, but CIU triaxial testing concluded that peak effective strengths fell somewhere near 20° and 10kPa cohesion.

2.3.2 Limit Equilibrium Analysis

Limit Equilibrium Analysis (LEA) was performed on various 2D cross-sections of the dam, using different failure surfaces, including circular and block failure modes, one of which is shown in Figure 2.9. Upon completion of LEA, it was determined that due to the strain-softening characteristics of the foundation material, LEA on its own was not sufficient to determine the instability of the dam, as a Factor of Safety (FS) of less than 1 was unachievable without accounting for the strain softening in the foundation and liquefaction of the tailings, which were modeled using peak effective stress parameters. However, indicative failure mechanisms obtained with the minimum FS were considered in [1] for reference, as indicated in Figure 2.9. Note that the failure is extending from the toe of the dam, before entering the tailings beneath the upstream construction phases, ultimately emerging somewhere behind the stage 1 buttress.

2.3.3 Small-Deformation Analysis

In addition to LEA, small-deformation numerical analysis was performed using the Finite Difference Method (FDM), through the use of FLAC in both 2D and 3D. The model is constructed using traditional mohr-coulomb to describe the dam materials. Through their

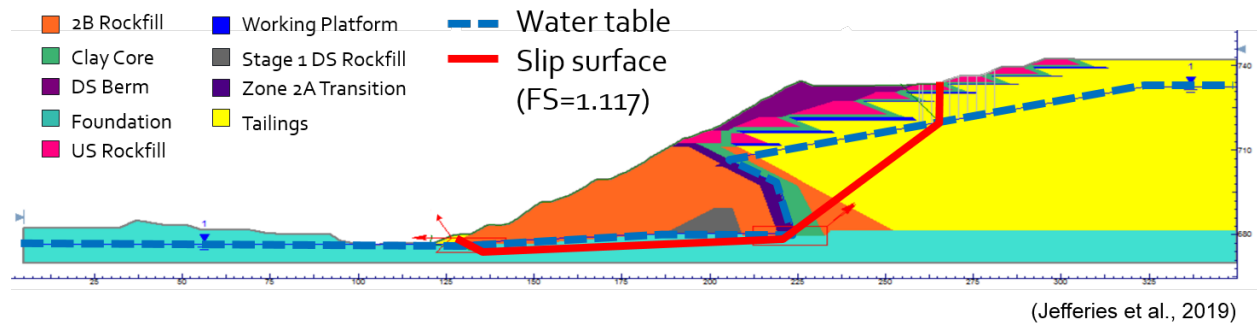


Figure 2.9: LEA Model modified from ITRB [1] to Model Potential Failure Surfaces

numerical analyses as well as previous information from the LEA, it was found that the properties of the clay core did not have a significant impact on the formation and location of the failure surface. CHSoil was used to model the initial behavior of the soil leading the peak strengths, to simulate the loss of stiffness as the soil approached peak strength, before the model was switched to a relationship which modeled the softening of the material to softened strengths. CHSoil required a calibration of the foundation material based upon the laboratory data, and as such three such tests were presented and the material was calibrated on these tests, with peak strengths of the foundation ranging from effective friction angles of 16-22°, and effective cohesion of 10 kPa. Residual effective friction angle varied with confinement, from 13-18°. NORSAND was used to describe the tailings characteristics, because of its capability of capturing a full range of the soil liquefaction, such as the static liquefaction of the loose tailings, or dilation in the case of denser soils. It is quite suitable and adept in this scenario for simulating the brittle collapse (i.e., flow liquefaction) behavior exhibited by the type of loose, contractive tailings present.

By simulating the progression of the construction of the dam through its many phases, it was observed that there was a thin band of the foundation layer which was softening towards its residual strength as construction progressed, indicating a progressive failure mechanism from the toe to the upstream side. This is illustrated in Figure 2.10, where the formation of

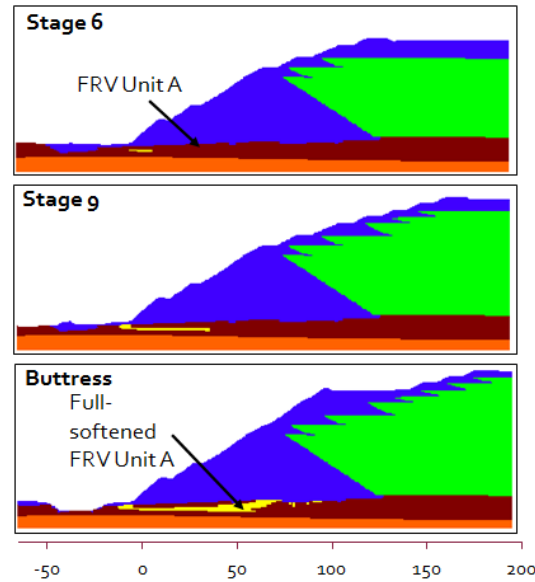


Figure 2.10: Numerical Conclusions modified from ITRB [1] Using FLAC: Visualization of Progressive Softening of Foundation Under Construction. Units in meters.

this shear band at different stages of the construction is indicated in yellow.

Additionally, the influence of the state parameter (ψ) in NORSAND, which is used to define the susceptibility of the tailings to liquefaction as a way of relating their behavior to the critical state line was examined in the ITRB Report [1]. Figure 2.11 presents the normalized stress instability ratio I (Eq. 2.1) of the tailings obtained in FLAC after the the two final stages of construction.

$$I = \eta/M_t \quad (2.1)$$

$\eta = q/p'$ is the predicted in-situ stress ratio (being p' and q the Cambridge stress variables) and M_t is the stress ratio of failure. When I approaches 1 indicates that the tailings are getting closer to the critical state. Figure 2.11 illustrates a transition of the tailings towards critical state just after the construction of the buttress. This provides a first estimation

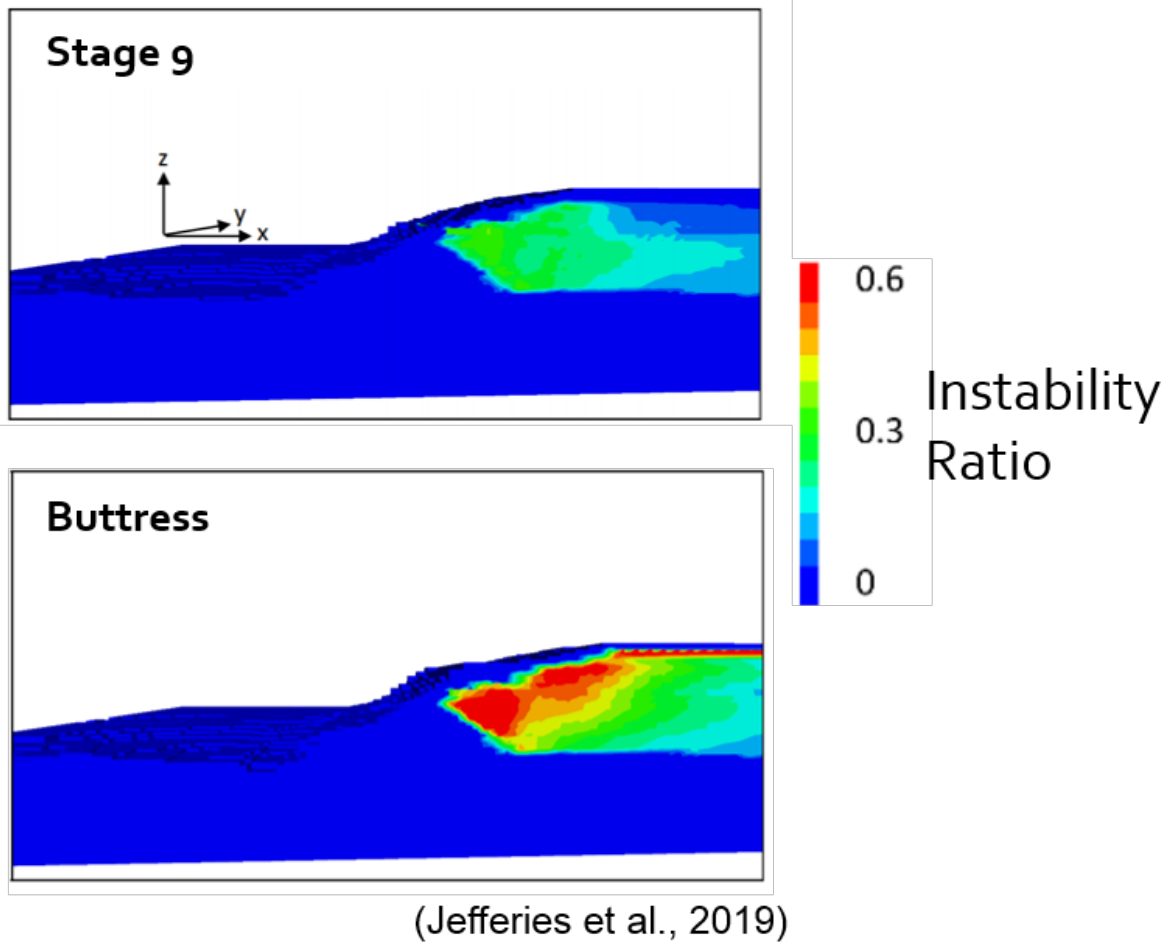


Figure 2.11: Numerical Conclusions Modified from ITRB [1] Using FLAC: Instability Ratio of Tailings at Final Two Stages of Construction

of the area that are more subjected to soften and liquefy (in red) especially in the case of a rapid (undrained) loading (i.e., resulting from the initiation of failure and consequent motion) when $M_f < \eta_{il}$.

An additional topic studied during the small strain analyses included the potential impacts of two earthquakes of roughly magnitude 3 the day prior to failure on liquefying the tailings. The data collected from the cyclic DSS tests was used, and it was determined that those earthquakes did not have an impact on the failure.

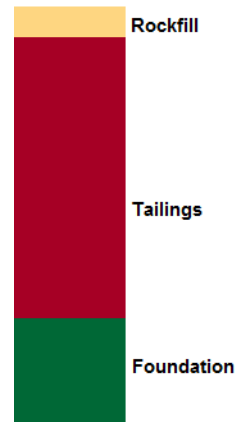


Figure 2.12: Simplified Boring Log of CE433 From Post-Failure Investigation

2.3.4 Runout Data

In order to validate the runout and large deformations obtained with the MPM numerical model presented in Chapter 4, it is essential to compare the results with reliable data. The available data on post-failure and final runout conditions presented in [1] includes final topography (Figure 2.8). The topographical measurements from this cross section are valuable in determining an expected final topography for our own model. Additionally, the movement of the Pump House (Figures 2.7 and 2.8), originally located near the toe of the dam serves to reinforce and provide further validation. Results from non-invasive soil testing methods (presented as the colored cross section in Figure 2.8) were found. Also, the boring log CE433 (indicated in Figure 2.8) has been considered. A simplified interpretation of CE433 is shown in Figure 2.12.

2.4 Causes of failure

The ITRB [1] was able to conclude that the progressive softening of the foundation layer under the dam as a result of the upstream construction combined with the following con-

struction of buttresses and excavation at the toe created initial horizontal movements of the dam. These horizontal movements meant the reduction of support for the tailings, and the contractive behavior of these loose, saturated tailings meant that as a result, they liquefied, leading to a reduction in resisting forces, ultimately causing the failure and runout observed.

Chapter 3

Material Point Method

This chapter is divided into three sections. The first section discusses what the Material Point Method (MPM) is and briefly describes how it works. In the second section, the reasons MPM was selected are presented. In the final section, several other uses for MPM within engineering application are given.

3.1 MPM Method

MPM is a continuum-based numerical method which allows for large deformations. It was initially proposed by Sulsky et al. (1994) [13], as a way of simulating large deformations in history-dependent materials. The ability to model under large strains by this method is important, as it does not run into issues which traditional Finite Element Methods (FEM) and Finite Difference Methods (FDM) run into, such as mesh entanglement, which limits them from running analyses with extremely large deformations. MPM addresses this problem by having a fixed mesh. MPM represents the materials of the model as a continuum with "material points". Each material point is representative of specific volume or areas of the material domain, move together with the material and carry all the information including e.g., mass, kinematic variables, material state variables, strains, and stresses. The MPM computational cycle is presented in Figure 3.1. The points underlay the computational mesh, and first, they share their information with the corresponding nodes of the mesh. At

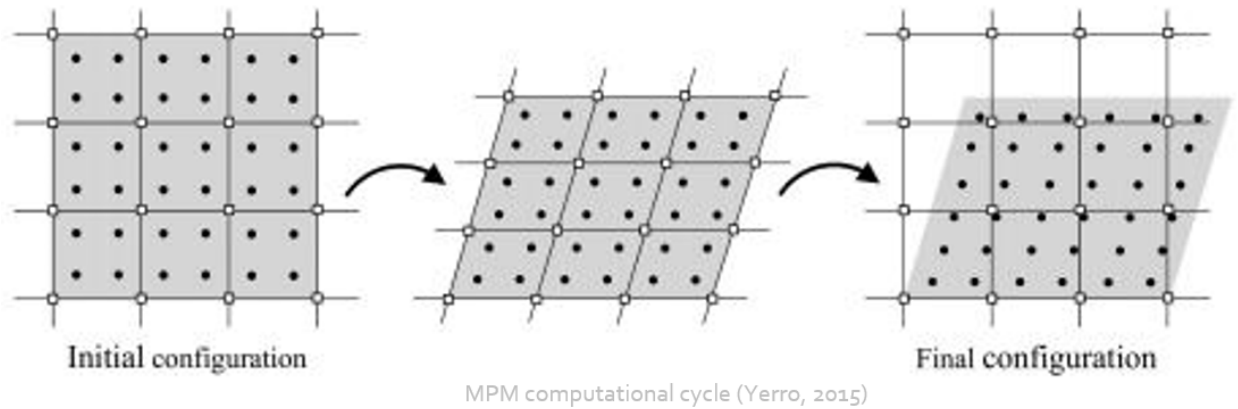


Figure 3.1: Graphical Representation of MPM Computation Cycle (from Yerro, 2015) [2]

the nodes, the dynamic momentum balance equations are solved and the nodal accelerations are calculated. This information is used to update the kinematic variables of the material points (i.e., velocity, displacement, location), as well as the state variables, strain, and stress. Finally, the mesh is reset and a new configuration of material points in the original mesh is encountered, ready to initiate the next time step. MPM was originally developed for one-phase materials but in the last 10 years, it has been extended for the modeling of hydro-mechanical coupling with two-phase (e.g., consolidation of saturated soils) [14] and even three-phase (e.g., unsaturated conditions) formulations [15]. Of particular interest to this paper are the one and two-phase formulations, as the model materials are treated as either being dry or fully saturated. This type of formulation has two common ways of addressing in traditional numerical methods, and is no different here: the water can be modeled as a separate continuum within the mesh, or it can be coupled to the solid material.

3.2 Reasons for Selection

Because of the unique behaviors of the many materials present in the failure, numerical simulations are necessary to appropriately model the dam-tailings-foundation system. Since

we are primarily interested in final runout and post-failure kinematics, typical numerical methods such as FEM and FDM cannot be used due to mesh entanglement problems at large strains. While similar methods to these could be employed where the mesh deforms, with the model remeshing periodically to remove entanglement issues, these other methods are more computationally expensive. Since the background mesh plays host to boundary conditions rather than the continuum of points, this enables the application of the boundary conditions to be somewhat easy. Additionally, since MPM resembles traditional FEM in many aspects, as the calculations are carried out at the nodes of the mesh, this allows knowledge from FEM to be more easily transferred to the method and simulations. For these reasons, MPM was selected to model our post-failure analysis.

3.3 Applications

The applications of MPM are varied. Early uses for MPM included such things as modeling of thin membranes, contact problems, and decohesion and delamination [2]. More direct applications to engineering, such as through the modeling of field tests to better understand soil-equipment interactions include the modeling of CPT such as by Beuth (2012) [16] and Ceccato (2012) [17]. Recently, MPM has been applied to better understand the behavior and interactions between soil and testing with regards to the application of the Free Fall Penetrometer (FFP) by Zambrano-Cruzatty et al. (2020) [18]. As early as 1999, MPM was applied to study the discharge of material from silos by Wieckowski et al. (1999) [19]. Coetzee et al. (2007) [20] and Mackenzie-Helnwein et al. (2010) [21] looked at the interactions of dragging, as well as excavation procedures through the use of MPM. Large scale deformations, and the application of anchors in soil modeled by MPM were presented by Vermeer et al. (2008) [22] and Wieckowski (2004) [23]. In 2013, Al-Kafaji applied the

MPM for the simulation of tunnel entrance collapse [24], while Mast presented the modeling of avalanches with structures [25]. Slope stability applications for MPM were studied and presented by Soga et al. (2016) [26], with more specific applications including the Oso Landslide of 2014 applying MPM, done by Yerro et al. (2019) [27], and the Aznalcollar dam failure of 1998 being presented by Zabala & Alonso (2011) [28].

Chapter 4

MPM Model

Chapter 4 is organized in the following manner. In the first section, we present the geometry and initial setup of our model. Next, the different materials and their constitutive models are presented. Finally, we discuss the calculation process by which the model is initialized and run. All the simulations are performed using the open source Anura3D software [29].

4.1 Geometry

The initial geometry of our model is constructed based upon a digitalization of the Cadia dam's cross section from the ITRB report [1], as seen in Figure 2.7. The model was divided into different materials, based upon water table (saturated vs dry materials), available liquefaction information (liquefied vs non-liquefied tailings), foundation data (FRVA, FRVB, pre-softened FRVA) [1]. The initial geometry for the reference MPM model is shown in Figure 4.1. The groundwater table is indicated with a dotted line. Note that the transition zone and clay core of the dam structure are not considered but the rockfill of the dam has been divided (yellow vs orange materials in Figure 4.1) to distinguish between dry vs saturated material. The liquefied tailings (indicated in green and red colors in in Figure 4.1) are assumed to liquefy, with delays between each zonation. The two green areas are the approximate area which was predicted to liquefy based upon the ITRB report [1], while the additional red area is an additional area needed to achieve the full runout. The area where

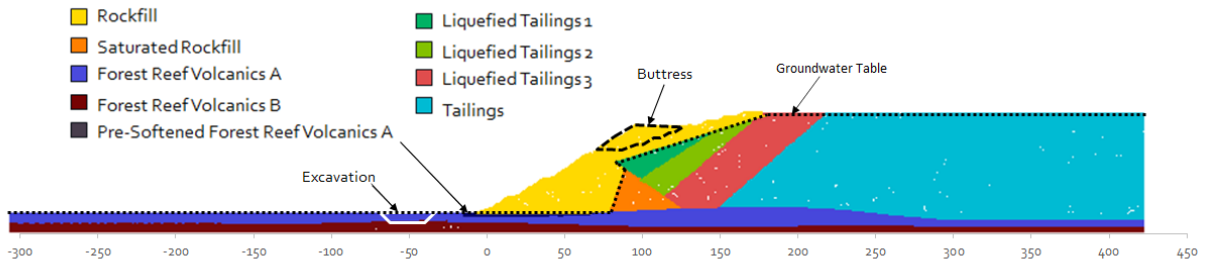


Figure 4.1: Reference Model Geometry (units in meters)

excavation occurred is shown, but is initially kept filled for stress initialization purposes.

The model is constructed using a fully-coupled hydromechanical MPM formulation for the saturated materials, while the material above the water table (i.e., dry rockfill) material is kept fully dry for the whole analysis. Boundaries preventing the escape of water and soil are present in the form of rollers on the top, left and right sides of the model, and as pins along the base of the model. The model's mesh cover the whole computational domain. It consists of triangular, linear elements, shown in Figure 4.2. The element sizes ranging from 1-3 m², each element initially hosting three material points in it at the start of calculations. Element size was selected to adequately provide a refined calculation network to prevent potential interference from an overly coarse mesh, while still being large enough so as to not cause calculations to be unnecessarily lengthy in time. Three material points per element were done to prevent the creation of empty elements during calculation embedded within material. The mesh elements are closer to 1 meter in size in the foundation due to the shear band present as well as the strain-softening characteristics of the material to provide a more accurate depiction of the behaviors there.

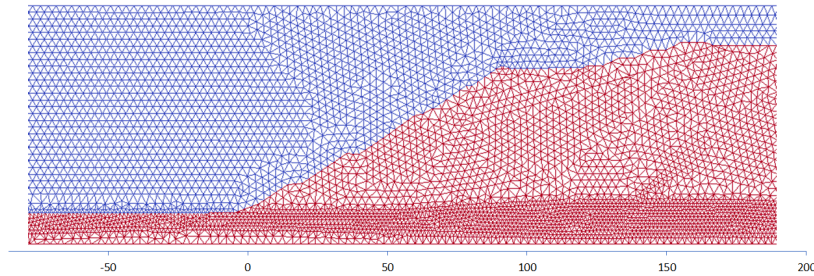


Figure 4.2: Computational Mesh of Model (units in meters)

4.2 Materials

The three broad categories of the model's materials (Dam, Tailings, and Foundation) are discussed in the following sections. The properties of these materials were defined by available lab tests whenever possible, and by literature review and examination of the ITRB's [1] own selection methods whenever laboratory data was not available.

4.2.1 Dam

As previously discussed in Chapter 2, there are three materials found in the dam. The ITRB noted that the properties of the rockfill and transition/filter material were fairly similar, and that the clay core did not provide a significant impact upon the failure mode and initiation [1]. For these reasons and for the simplicity of the numerical model, these materials were taken as a single, homogeneous material when modeling the dam. The rockfill of the dam is still modeled as two separate materials to allow for the water table to be defined. These materials exhibit the same properties, with the exception being the saturation of material below the water table. Saturated rockfill is defined as a fully-coupled saturated material, while the dry rockfill is modeled as a dry material. The strength profiles are modeled using Mohr-Coulomb failure envelopes. The element size in the rockfill is approximately 3 m²,

Material	Porosity	Density [kg/m ³]	Young's Modulus [MPa]	Poisson's Ratio	Cohesion [kPa]	Friction Angle
Dry Rockfill	0	2000	78	0.35	0	40
Saturated Rockfill	0.29	2400	78	0.35	0	40

Table 4.1: Rockfill Characteristics

selected to be refined enough such that the coarseness of the mesh does not interfere with failure propagation, but still allows the code to run efficiently. Table 4.1 shows the values selected to model this material.

An effective friction angle of 40° was selected, and was found to be consistent with the ITRB report [1]. A selected Young's Modulus of 78 MPa was selected, based on review of the ITRB report [1], as well as further review in [9] and [10], which was found to be consistent with expected values. Unit weight of 2000 kg/m³ was selected as a typical unit weight, as it was found by the ITRB to vary from 1900-2000 kg/m³ [1].

4.2.2 Tailings

Tailings of the dam are composed of a silty-sandy material susceptible to liquefaction. Due to current limitations in modeling software, advanced soil models such as NORSAND are not available in the Anura3D code as of yet. Because of this, the tailings are modeled using the Mohr-Coulomb failure effective envelope for when the tailings are not liquefied, with the model artificially switching over to an undrained strength (S_u) Mohr-Coulomb model for the simulation of liquefied tailings. This simplified procedure is required because the Mohr-Coulomb criterion is a simple model that cannot intrinsically simulate the contractive behavior of the tailings and consequent liquefaction process. This means that in the model, we need to prescribe what are the liquefied tailing zones (controlled by residual undrained shear strengths) and at what moment in time are being liquefied. This is the most important

Material	Porosity	Density [kg/m ³]	Young's Modulus [MPa]	Poisson's Ratio	Cohesion [kPa]	Friction Angle
Default Tailings	0.5	3020	81.5	0.2	0	34
Liquefied Tailings	0.5	3020	81.5	0.2	10	0

Table 4.2: Tailings Characteristics

uncertainty of the model proposed here. In the reference model (Figure 4.1), the extension of the liquefied tailings has been determined after an iterative process by comparing with topographic and field data. A brief summary of this calibration process is presented and discussed in Section 5.3.

The material properties are shown in Table 4.2. Tailings effective stress friction angles are based upon ICU Triaxial tests, and ranged from 34-40°. For simplicity, 34° was selected as the drained in-situ strength of the tailings. Additionally, these values were adopted when evaluating the dam in design during expansion in 2017 [1]. The liquefied, undrained strength of the tailings was selected as 10 kPa. Further examination is performed to examine the increase of undrained shear strength with depth (about 5 kPa for every 10 meters of depth), giving a range of about 3-30 kPa for the undrained shear strength of the liquefied tailings. A Poisson's ratio of 0.2 was adopted based upon recommendations outlined in the ITRB report, and is considered representative of the tailings. The Young's Modulus of the tailings was obtained using seismic dialometer testing in the area near the slump, and was found to vary with depth from roughly 20-144 MPa, and as such an average value of 81.5 MPa was used for the model.

The Poisson's Ratio of the liquefied tailings remains the same between the default and liquefied tailings, as the tailings are still simulated using effective stress parameters, and when strength is measured in cohesion without friction the maximum stresses remain the same. A value of 0.2 was selected, in accordance with the findings by the ITRB [1].

4.2.3 Foundation

As presented in Chapter 2, the foundation in the area of failure is a residual clay of varying thickness, the result of weathering of the in-situ basaltic rock. This clay is subdivided into two units FRV Unit A (FRVA) and FRV Unit B (FRVB). The upper layer, FRVA exhibits strain-softening tendencies, which is not exhibited by the FRVB. There is a great deal of scatter in the peak and residual strengths of FRVA from lab tests. Figure ?? shows this scatter, where the peak strengths at the same confining stresses show a very visible amount of variability, possibly due to inconsistent weathering of the in-situ rock. DSS and ICU tests were performed on these materials under differing confining stresses, based on these results, FRVB is assumed to be in peak conditions.

Because of the complexity of the softening characteristics of FRVA, it becomes necessary to calibrate and refine a model for the soil. The soil is modeled using a Mohr-Coulomb failure envelope with strain softening, where the strain softening behavior is defined by the following exponential expressions:

$$c = c_r + (c_p - c_r)e^{\eta\varepsilon_p} \quad (4.1)$$

$$\phi = \phi_r + (\phi_p - \phi_r)e^{\eta\varepsilon_p} \quad (4.2)$$

Equation 4.1 defines the cohesion of the soil at specific strains, where η is referred to as the shape factor, and is used to define the rate at which the cohesion changes with strain. c_r and c_p are the residual and the peak cohesions, respectively, and ε_p is the amount of strain where the soil is being strained at stresses greater than the peak stress. Equation 4.2 defines the friction angle of the soil at strains, with much of the nomenclature remaining the same, where ϕ_r and ϕ_p are the residual and peak friction angles, respectively. In order to calibrate the model, it becomes necessary to choose a test representative of the failure.

To adequately simulate the strain-softening behavior of the foundation, the stress-displacement relationship measured in one of the DSS tests was numerically modeled. The test's confining stress was 1000 kPa, selected as representative of the stresses experienced by the foundation under the dam.

The selected test was digitized and used as a means of calibrating the rate at which the material reaches residual conditions, in order to accurately simulate the softening characteristics. The calibration's purpose is to determine the shape factor, η , such that the energy expended to achieve large deformations is the same for simulated and laboratory data. The general procedure for calibrating the shape factor is as follows:

1. Select a large strain laboratory test and its results. (In this case, a DSS test.)
2. The calibration is sensitive to mesh size, as such, the strains of the lab test need to be converted to distance based on an appropriate mesh size for the model. Thus, the lab test will be plotted with stress on the y-axis, and distance on the x-axis.
3. A digital laboratory test model must be constructed, with element sizes the same as will be in the simulated model.
4. The digital test is then run, and representative points are plotted with their deformation against stress, and plotted on top of the laboratory test.
5. The area under the two curves should be the same at large deformations, meaning the energy expended to achieve large deformations are the same. If they are not, the shape factor must be changed and another digital test is run. Otherwise, use the parameters used in the digital test for the model.
6. Note: If the mesh size must be changed for any reason, the shape factor will need to be recalibrated, as it is very sensitive to mesh size.

Using the above procedure, often referred to as a smeared-crack modeling (which negates the need to know the orientation of the failure plane), the shape factor was determined to be 120. The laboratory test used to calibrate is shown in Figure 4.3, shown in black. Note that the final stress measured in the test was taken as the residual strength, despite not leveling off (due testing constraints only allowing for strains of up to approximately 20% strain), and is indicated by the dashed line. This assumption almost certainly will over-predict the fully-softened strength. The numerical model calibration results are shown with the red line, with an element size of 1 m², and as such the simulated DSS test has a height of 1 meter. While the curves do not lay overtop one another perfectly as anticipated, the area beneath the two curves at large strains is the same, making the model a good fit for large displacements, which we are primarily interested in. By nature of the smeared-crack modeling procedure, the exact location of the failure plane need not be known for the test either. The Young's Modulus was taken as 39 MPa, as deemed reflective enough of the material based on previously simulated laboratory tests by the ITRB [1].

While a direct shear test or ring shear test might be more desirable for obtaining a true residual strength of the clay, because the samples using those tests were remoulded, the curves for these tests would not have adequately captured the evolution from peak to soft conditions, nor even have captured peak conditions appropriately.

In addition to the two zones FRVA and FRVB, there is another area of foundation material present in our model. Since the model begins at the point of failure, the area which softened progressively during construction is prescribed with a different material, and modeled in purely residual strength conditions with the standard Mohr-Coulomb, with an effective friction angle of 11.3° with no cohesion.

Table 4.3 summarizes the soil properties, as well as provides the shape factor, η , which was found in the calibration.

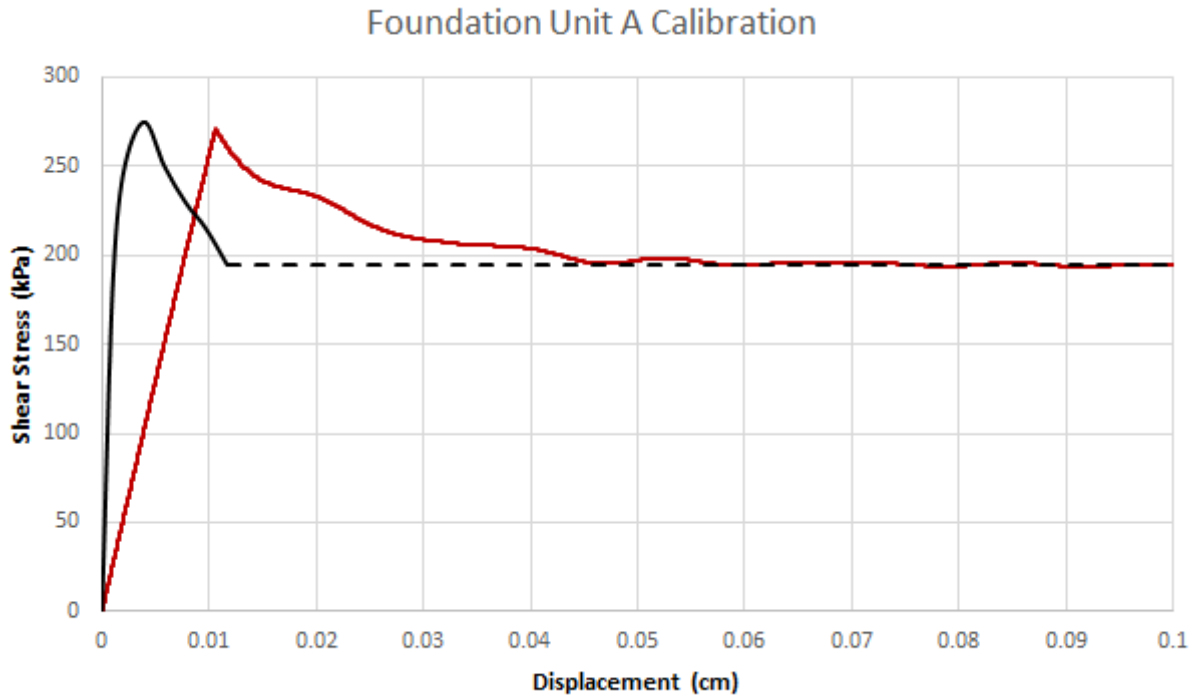


Figure 4.3: Calibration Plot of FRVA

4.3 Calculation Phases

Because the investigation is focused primarily on post-failure kinematics and the final runout, the model's simulation begins at the time of failure initiation. As such, the model is run using the following stages of setup and initialization, ultimately leading to the final runout:

1. Gravity is initialized under quasi-static conditions. Materials are kept in elastic con-

Material	Porosity	Density [kg/m ³]	Young's Modulus [MPa]	Poisson's Ratio	Peak Cohesion [kPa]	Peak Friction Angle	Residual Cohesion [kPa]	Residual Friction Angle	Shape Factor
FRVA	0.45	2824	39	0.3	10	22	0	11.3	120
FRVB	0.45	2824	39	0.3	10	22	N/A	N/A	N/A
Residual FRV	0.45	2824	39	0.3	N/A	N/A	0	11.3	N/A

Table 4.3: Foundation Characteristics

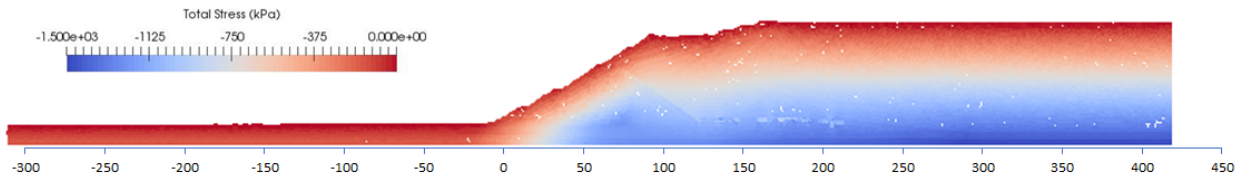


Figure 4.4: Stress Initialization: Total Vertical Stress

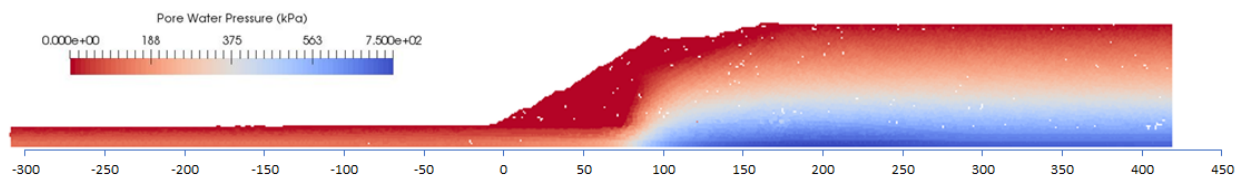


Figure 4.5: Stress Initialization: Pore Water Pressures

ditions. This stress initialization is checked to verify that the total stresses and pore water pressures initialized properly, as is shown in figures 4.4 and 4.5. As is shown, the pore water pressures increase as expected with depth based upon water table information. Additionally, the total vertical stress also increases as expected. Note that the software presents compressive stresses as negative.

2. The material constitutive models are switched to more realistic models (e.g., Mohr Coulomb and Mohr Coulomb with strain softening) and peak strength parameters are initialized. The model is allowed to run again for another load step to ensure solution convergence, once again checking to verify that stresses continue to behave as expected.
3. The pre-softened zone of the foundation material determined from previous numerical analyses is reduced to its residual strength, and the model is allowed to proceed to the next load step. At this point, the stresses are assumed to be close to those in the field just before failure.

4. At this point, the failure is triggered by excavating the part of the FRV Unit A near the toe (mimicking field conditions) and the first zone of the tailings (dark green material in Figure 4.1) are artificially reduced to their residual undrained shear strengths.
5. After five seconds from failure initiation, the undrained shear strength of the "next" zone of tailings (light green material in Figure 4.1) are artificially reduced to their residual undrained shear strengths. Because of the uncertainty with the timing, a parametric analysis was performed to study the effect of this timing, with the five seconds serving as a reference case.
6. Finally, the last zone of tailings (red material in Figure 4.1) is liquefied, ten seconds after failure initiation. The calculation is allowed to continue until the new stable configuration is reached (when the dam stops moving, and the tailings behind it are no longer failing). At this point, the final runout is identified.

Chapter 5

Results

Chapter 5 presents the results of the reference model and of a series of parametric analyses designed to examine the influence of different model characteristics on the final runout. It is organized in the following way. First, the results from the reference model are compared with the final topography and boring data from the field. Second, the evolution of the post-failure mechanism and kinematic behavior is presented. Third, the influence of the tailing properties and liquefaction extent is discussed and compared with the reference model by means of a parametric analysis. Then, the influence of the foundation's brittleness is examined through parametric analysis. Finally, the influence on the post-failure runout of the presence of the toe excavation and the buttress from the last construction stage (Stage 10) are examined and discussed.

5.1 Comparison of the reference model with topographic and field data

The final geometry obtained with the reference model is shown in Figure 5.1. Note that material properties and geometry is based on topographic, field, and laboratory data presented in [1], but the most important uncertainty is the extent of the liquefied tailings. Note that the reference model presented in this section has been calibrated in order to fit the final

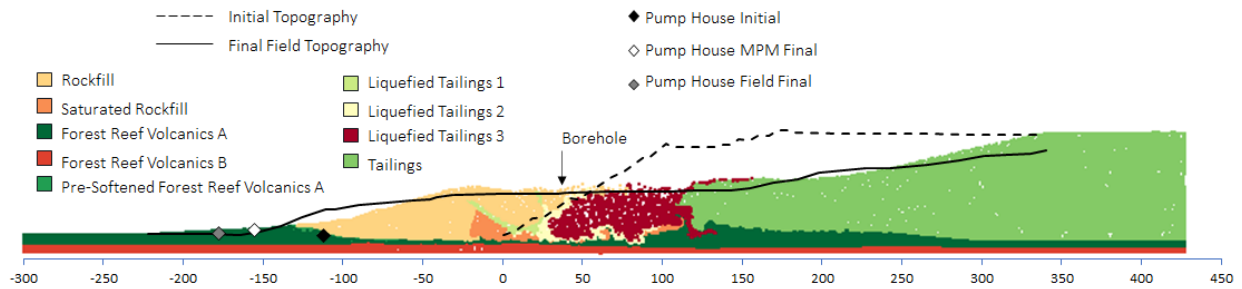


Figure 5.1: Final Runout: Reference Model (units in meters) [Model 1]

runout observed in the field. A good fit is observed when comparing the final topography obtained with the reference model and the one obtained from field data. In Figure 5.1, the initial topography is also represented for reference in a dashed line.

Apart from the topographic profile, two additional metrics are used to validate the performance of the numerical model. The first one is through the movement of known points, such as the pump house, which is also indicated in Figure 5.1. While it does not fully reach its final location, it is within approximately 10 m, which is a fair match. The second metric is through the comparison of a borehole from the field (CE433), with the corresponding digital borehole from the same location relative to the initial geometry. Both boreholes are compared in Figure 5.2, and while there are minor differences between the two, namely a slight increase in depth of rockfill and depth to the foundation, they show an acceptable match.

A final metric which could be considered is the non-invasive testing cross section presented in Figure 2.8, which could indicate a larger extent of tailings beneath the surficial dam material. However, due to the uncertainty associated with this type of testing in determining the materials in this way, it was determined to be an unreliable metric to verify the model with.

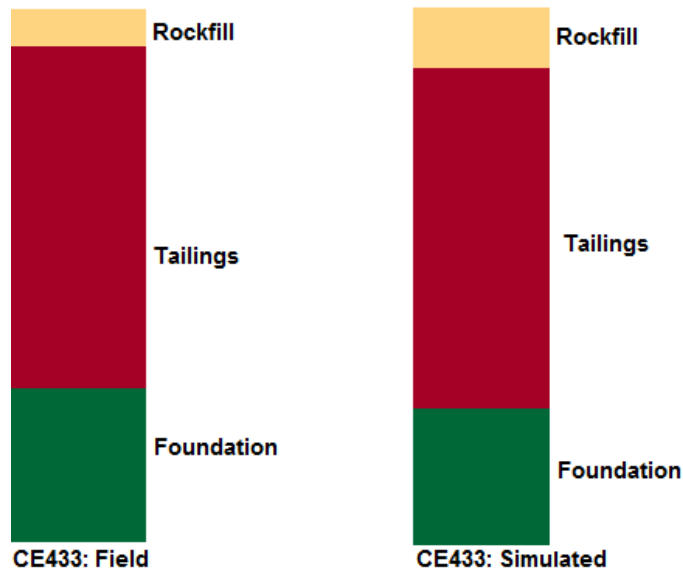


Figure 5.2: Digitized Borehole Comparison

5.2 Post-failure mechanism and kinematic behavior of the Cadia dam failure

Figure 5.3 presents the evolution of the failure mechanism in terms of deviatoric shear strain. Just after the failure triggering, the strains localize in the foundation FRVA unit as a result of the softening behavior and quickly progress horizontally. Before reaching the tail of the first phase of the dam, the failure mechanism deviates towards the liquefied zone at an angle of approximately 40° until reaching the ground surface. The shape of the initial failure mechanism is consistent with the failure plane predicted by [1]. After that, the failure mechanism evolves. The interface between the foundation and the tailings begins to strain, and a retrogressive failure initiates behind the dam, with new shear bands forming within the tailings. This ultimately causes the final topographic profile. From Figure 5.3 it is important to emphasize that the analysis of post-failure behavior is complex as a result of

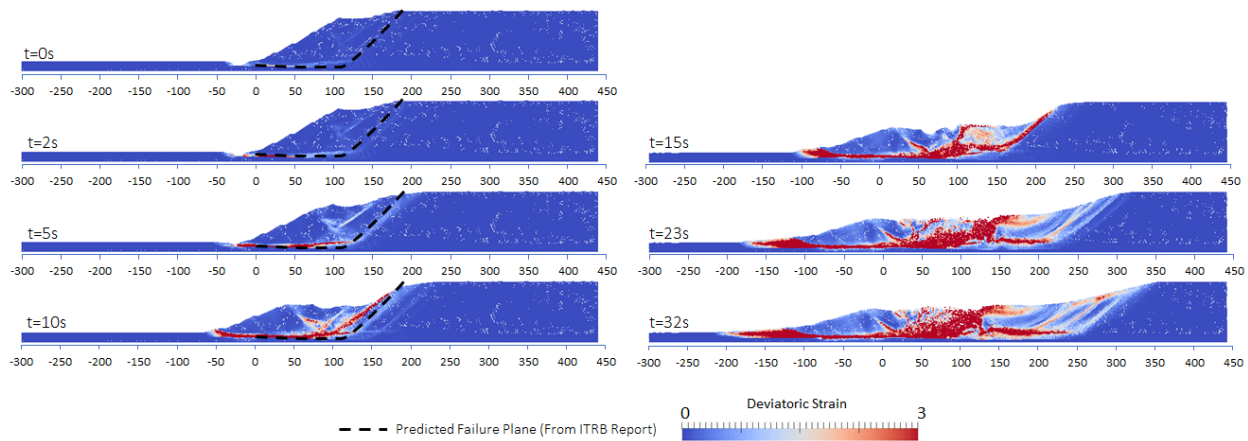


Figure 5.3: Failure plane progression through deviatoric strain at different times after the failure triggering (distance in meters)

the multiple failure mechanisms developed as the motion evolves and geometry changes in time.

Figure 5.4 shows the velocity field at different times during the instability process. Note that the Anura3D software used to perform these analysis is fully dynamic and all inertial terms are considered in the calculation. Initially, the dam fails by mobilizing along the failure surface predicted in the ITRB report [1]. As time passes, the dam begins to stabilize (eventually fully stabilizing), while the tailings behind it are continuously being mobilized as a result of a retrogressive failure mechanism. Note that this kinematic behavior indicates that the amount of tailings mobilized behind the dam will eventually no longer impact the final runout of the dam. Finally, a new equilibrium is reached around 35 s after the failure triggering. After that, the final topography remains constant. Minor numeric instabilities are noted in the zone of liquefied tailings as a result of the explicit time integration scheme, but they do not impact the final runout and topography. The failure can be classified as "Very rapid" since the maximum velocity is around 4.5 m/s (just below 5m/s).

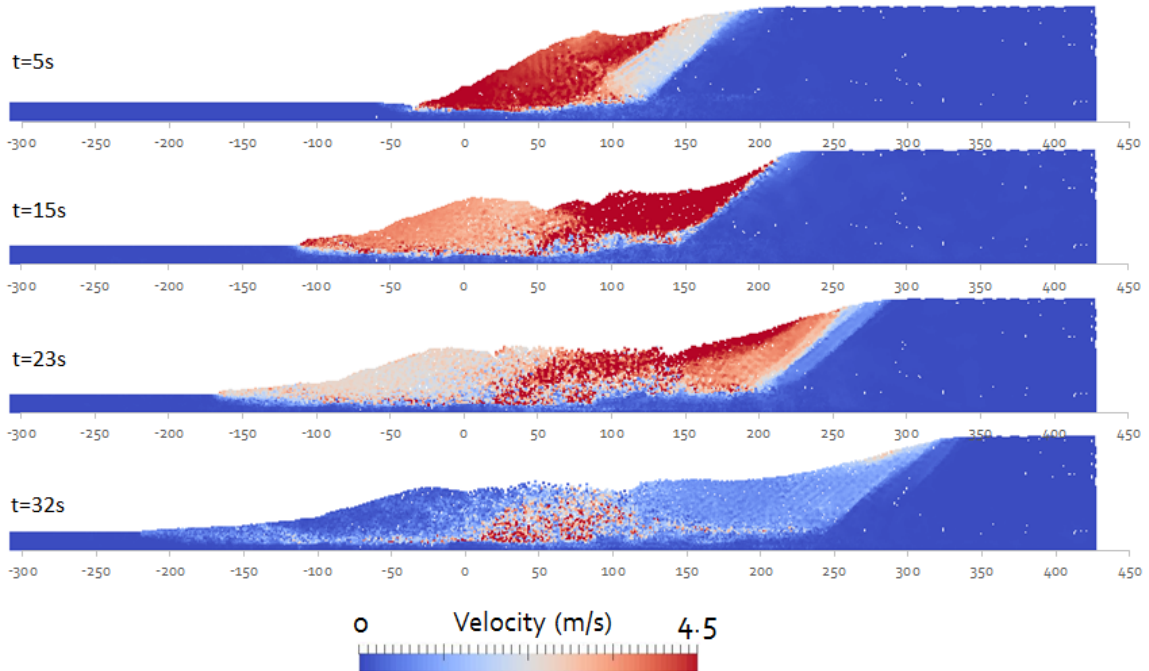


Figure 5.4: Reference Model with Velocity Plotted at Various Times (distance in meters)

5.3 Influence of the tailings

The tailings became an important target of examination for their influences on the final topography and runout as a result of intrinsic uncertainties and simplifications considered in the reference model. This section is broken down in three subsections to separately study the effect of (a) the extent of the liquefaction, (b) the rate at which the tailings liquefy, and (c) the strength of the liquefied tailings.

5.3.1 Liquefaction Extent

The extent of the liquefaction of the tailings plays a key role in the runout of the dam. Without liquefaction, the dam falls far short of what could be expected for a final runout or topography. However, after a certain point, the amount of tailings which liquefy matters

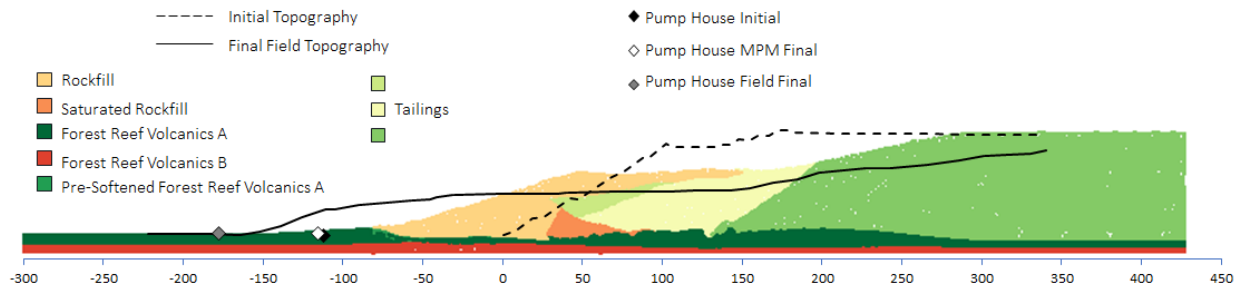


Figure 5.5: Final Runout: No Liquefaction (units in meters) [Model 2]

significantly less after a certain threshold is passed.

In Figure 5.5, 5.6, and 5.7, liquefaction was changed in the following ways. In Figure 5.5, the tailings were not liquefied. The runout is clearly reduced, with the toe of the dam only traveling 70-80 meters, while the reference point (i.e., the pump house) barely moves. It is clear from this that susceptibility to liquefaction plays a key role in the final runout. The next simulation, shown in Figure 5.6 reinforces this notion, by allowing the small area of tailings shown in pale green to liquefy at failure initiation, causing the dam to move a further 20 meters, as well as motivating the reference point to move. Even a small amount of liquefaction enables the dam to move notably further. Finally, Figure 5.7 adds a fourth zone of tailings which are allowed to liquefy. It can be seen that when compared to Figure 5.1, the runout are the same, which implies and reinforces the notion that the retrogressive failure of the tailings no longer influences the movement of the dam after a certain point, as it stabilizes.

5.3.2 Rate of Liquefaction Triggering

The next topic of interest regarding the influence of the tailings is the rate at which the different zones of liquefying tailings are triggered. Two cases were chosen to study the

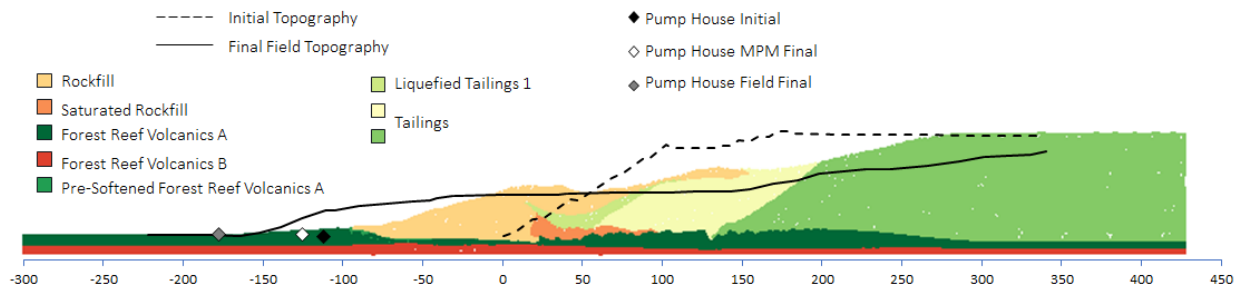


Figure 5.6: Final Runout: First Zone Liquefies (units in meters) [Model 3]

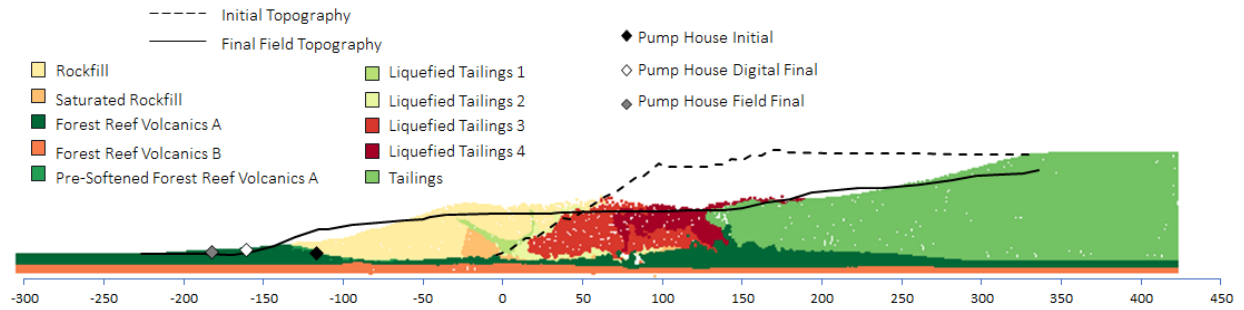


Figure 5.7: Final Runout: Fourth Zone of Liquefaction (units in meters) [Model 4]

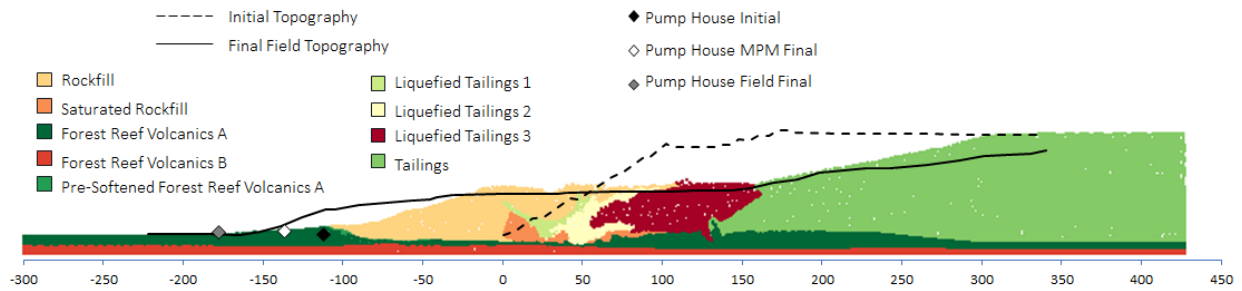


Figure 5.8: Final Runout: Reduced Rate of Liquefaction, 10 seconds Between Liquefied Zones (units in meters) [Model 5]

impact of this. In the first case, the tailings are liquefied more slowly, with each zone of tailings liquefying 10 s apart, instead of 5 s as in the case of the reference model. The results of this are shown in Figure 5.8. It is visible that the runout of the dam is slightly reduced with respect to the one obtained with the reference model (Figure 5.1), by about 30 m.

The other case is the instance where all liquefying zones liquefy at once, at failure initiation. The runout for this case is seen in Figure 5.9. In this case, the movement of the slope is almost 20m more, and the results fit really well the field data. Note that the reference point (i.e., the pump house) almost perfectly overlies the actual field location.

The conclusion of these results are relevant because they show the influence of the rate of liquefaction in the post-failure analysis and encourage future research to include a more advanced constitutive model capable of more accurately represent the behavior of the tailings and predict the liquefaction initiation.

5.3.3 Liquefied tailings Strength

Finally, the influence of the liquefied strength of the tailings upon the final topography was examined. As explained in Chapter 2, the liquefied strength of the tailings is dependent

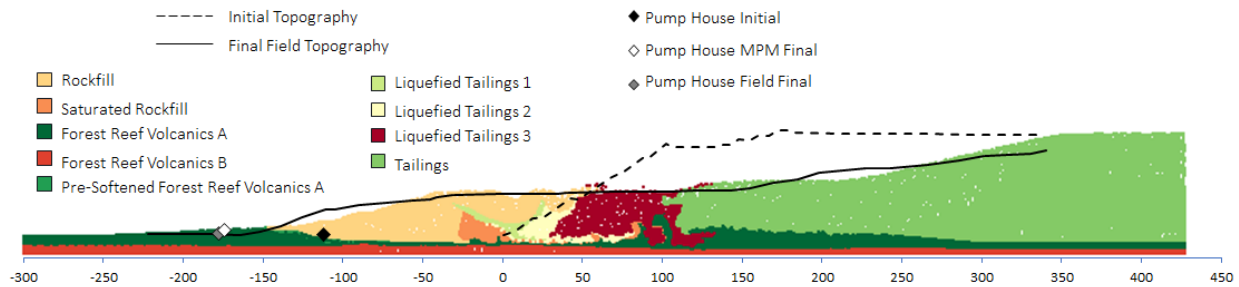


Figure 5.9: Final Runout: All Zones Liquefied at Failure Initiation (units in meters) [Model 6]

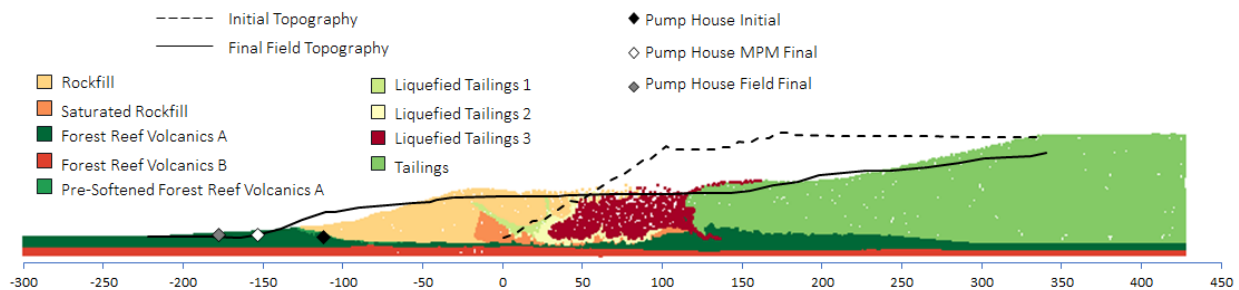


Figure 5.10: Final Runout: Low Liquefied Tailing Strength (3 kPa) (units in meters) [Model 7]

upon confining stress prior to liquefaction. A variation of the liquefied undrained strength is expected to range from approximately 3-30 kPa across the profile, based upon CPT data. For simplification purposes, the reference model considers a constant undrained shear strength of 10kPa. To study the effect of this assumption, three other simulations are run to study the impact of the tailings' liquefied strength on the final topography.

When the tailings are homogeneously liquefied at their lowest liquefied strength of 3 kPa, the runout is barely effected, as seen in Figure 5.10. The reference point is also not significantly impacted, with both the final runout of the toe and the reference point moving an additional 5 m.

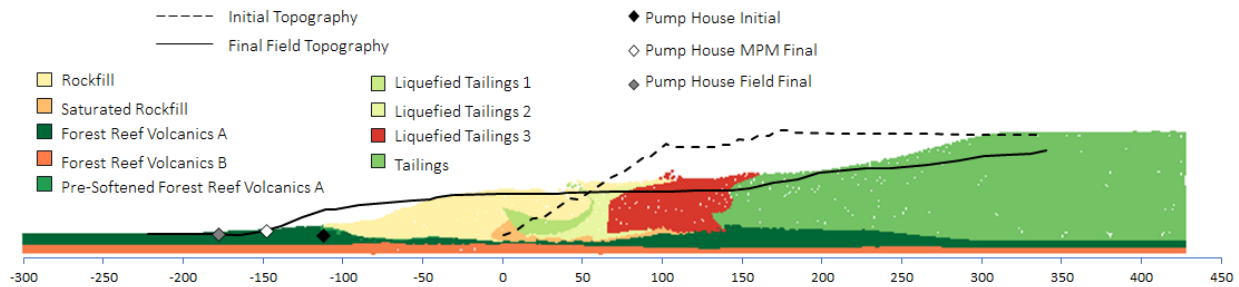


Figure 5.11: Final Runout: High Liquefied Tailing Strength (30kPa) (units in meters) [Model 8]

If the tailings are instead at their maximum liquefied strength of 30 kPa (corresponding to the deeper and more confined tailings), the runout is slightly reduced, as shown in Figure 5.11. The runout is reduced by approximately 10 m, and the movement of the reference point is not significantly impacted.

One final case was examined where the tailings are subdivided to account for their liquefied strength variation with depth, with their strengths relating directly to their initial confining stresses. The results of this simulation are shown in Figure 5.12, where it is clear that the impact of varying the liquefied strengths has little to no influence on the final location of the final topography either, almost matching the reference topography aside from some minor variations behind the dam.

5.4 Influence of the brittle foundation

The influence of the foundation's brittle behavior on the dam's runout was the next point of interest. This was handled under three different circumstances. The first model did not include strain softening, keeping the foundation (FRVA and FRVB) in peak conditions only. This case is equivalent to a theoretical case where FRVA is not pre-softened during the

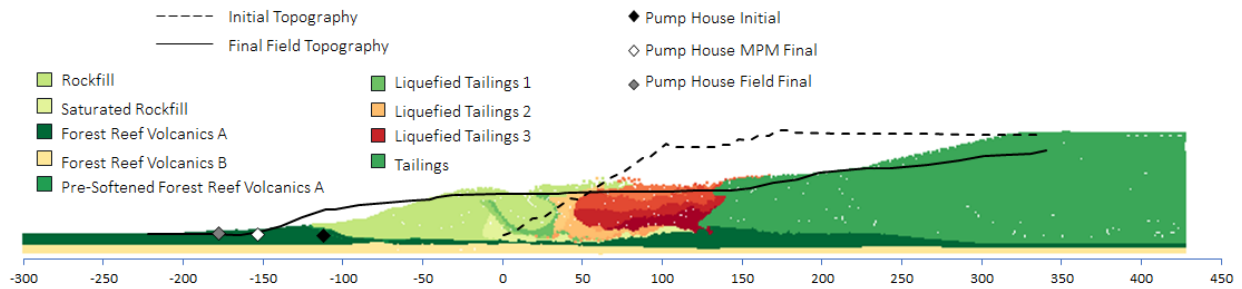


Figure 5.12: Final Runout: Varied Liquefied Tailing Strength with Depth (units in meters) [Model 9]

construction process. The rest of the model remains the same as the reference case, so the liquefied tailings could be triggered by an earthquake of significant enough magnitude. The results are presented in Figure 5.13. The dam as a whole does not slide forward in this case, and the runout is much less, with a more overtopping-type of failure mode, which is shown by the strain progression in Figure 5.14. The instability does not reach the reference point (i.e., Pump house), hence it doesn't move forward.

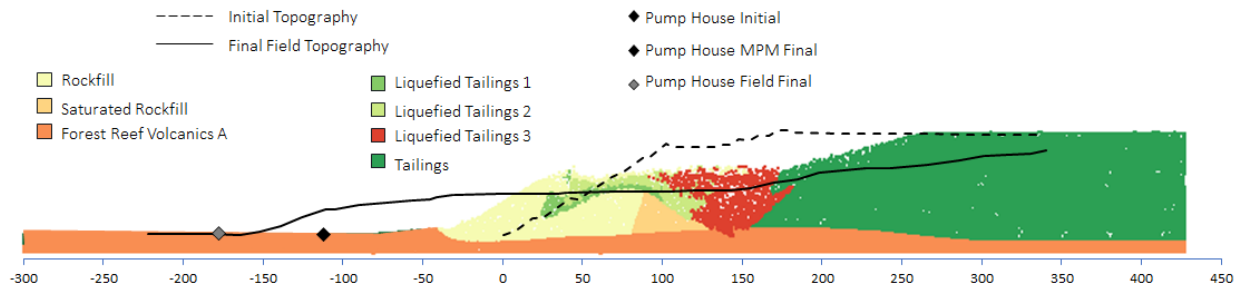


Figure 5.13: Final Runout: No Strain Softening in FRV (units in meters) [Model 10]

The next model gives FRVB of the foundation the same properties as FRVA, allowing for strain softening to occur at deeper depths. As presented in Figure 5.15, the runout is not strongly impacted by this when compared to the reference model. It does, however, have an

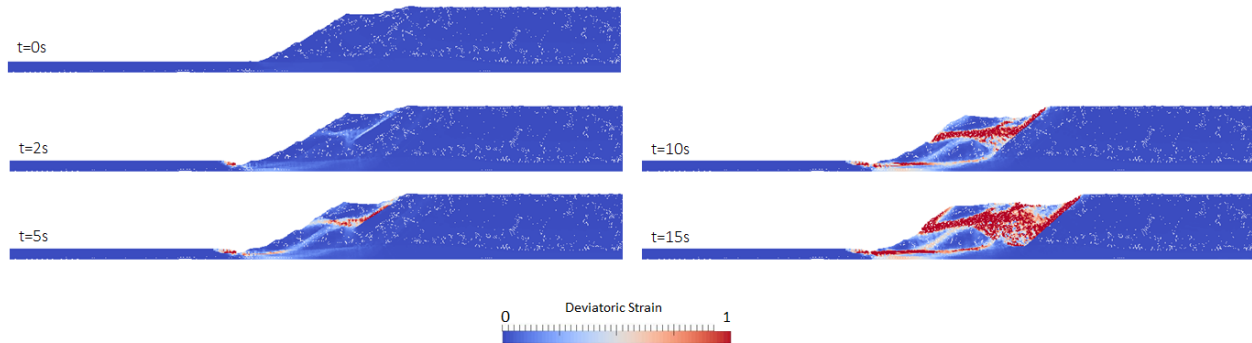


Figure 5.14: Failure progression through deviatoric strain at different times of failure with no strain softening

impact on the movement of the reference point of the pump house, resulting in a reduced distance traveled.

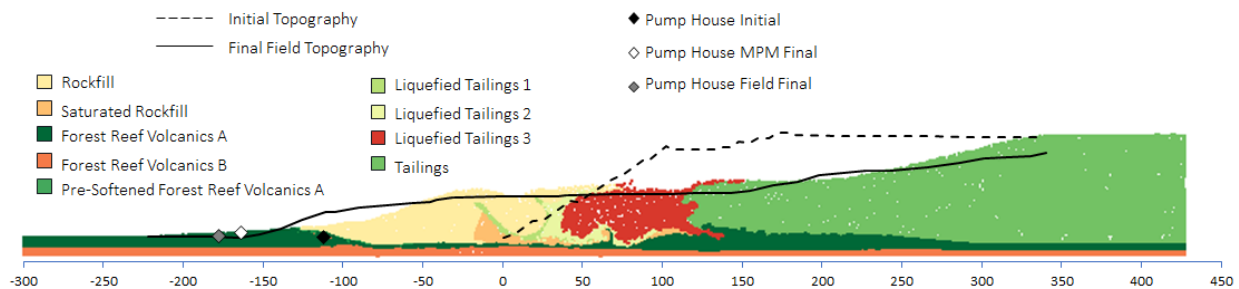


Figure 5.15: Final Runout: Strain Softening Included in FRVB (units in meters) [Model 11]

Finally, the model is run, using a lower residual strength in the FRVA, as could possibly be the case based upon previous comments on the test being calibrated, noting the residual strength plateau had not yet been achieved. The results of this model are shown in Figure 5.16. It is clear that this increases the runout of the toe by 20-30 meters, as well as pushing the pump house reference point past the final field location, which is expected given the lower residual strength of the foundation.

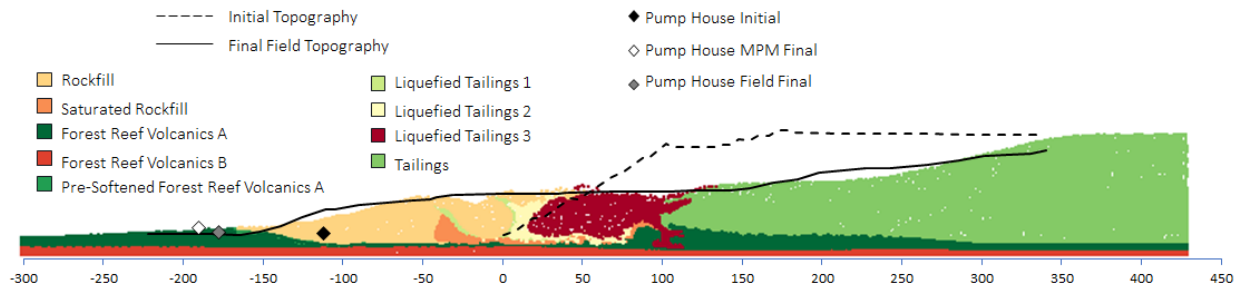


Figure 5.16: Final Runout: Reduced Residual Strength in FRVA (units in meters) [Model 12]

5.5 Influence of excavation and buttress (Stage 10)

Finally, another factor which was examined to determine its influence on the runout and failure was the geometry of the dam and foundation itself as a result of the construction of Stage 10. The model presented in this section is identical to the reference one but the initial topography corresponds to the end of Stage 9. This means that there is no excavation in front of the toe of the dam and the most recent additional buttress is not included. The results are presented in Figure 5.17. The dam moves roughly 85 m, significantly less than if the buttress and excavation were to occur. This is indicative of the dominance of the excavation on runout, as the excavation creates a empty space into which failed material can rush and continue through on its path downstream. The buttress also increases the inertia of the dam.

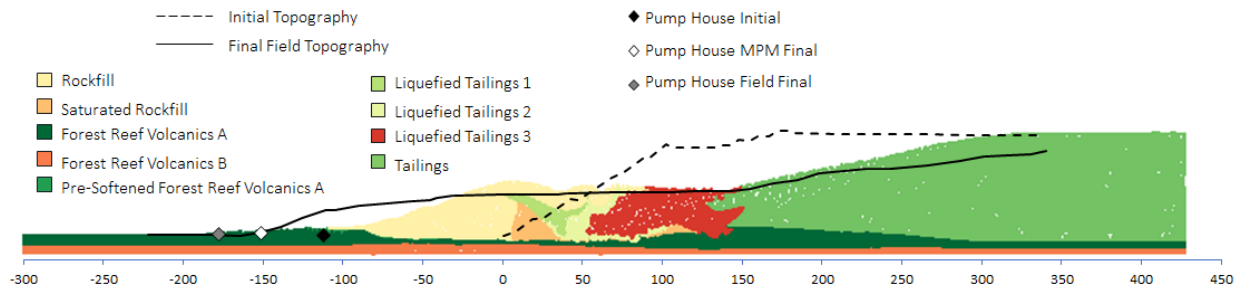


Figure 5.17: Final Runout: No Buttress Constructed, No Excavation & Tailings Liquefy (units in meters) [Model 13]

Chapter 6

Conclusions

The conclusions drawn by the previous analyses of the Cadia dam failure are presented in this chapter, starting with a re-examining of the importance of applying knowledge from a standpoint of risk management coupled with increasing safety concerns around tailings dams. Specific conclusions on material influences on the failure and runout are presented and summarized. Finally, future work and improvements for MPM that would enhance the work presented in this thesis are discussed.

6.1 Safety & Importance

With the continued rise of the catastrophic failure rate among tailings dam failures, there is a need to understand and manage risks associated with potential failure, such as could occur through material variability, construction practices, or earthquake induced liquefaction in these facilities. The latest call by the United Nations to reduce the consequences of failure on the local population and the environment to zero in the event of failure [5] highlights and reinforces the concept of this need. MPM adds value as a means of better understanding the post-failure behavior of tailings dams as well as the influences of different material properties and geometries, due to its unique capabilities of modeling large-strain problems, while allowing for concepts of traditional FEM to be easily transferred due to similarities between the methods.

Model Number	Changes	Toe Runout Distance (meters)
1	Reference	135
2	No Tailings Liquefaction	80
3	1 Liquefying Tailings Zone	95
4	4 Liquefying Tailings Zones	135
5	Reduced Liquefaction Triggering Rate	105
6	Increased Liquefaction Triggering Rate	155
7	Reduced Liquefied Strength	135
8	Increased Liquefied Strength	125
9	Varied Liquefied Strength with Depth	130
10	No Strain Softening	45
11	Strain Softening to Depth	130
12	Reduced Foundation Residual Strength	170
13	No Phase 10 Construction, Liquefaction of Tailings	85

Table 6.1: Summary of Simulation Runout Results

6.2 Material Influence

The interaction of the materials of and around the dam play out in varied ways. The model presented as the reference model exhibits good matching with final runout topography and field testing results. Presented in Table 6.1, the influence of the different material properties can be correlated with the runout distance, measured as the furthest distance the dam travels from its initial toe location.

It is clear from the tabulated information that some of main contributors to the runout are the residual properties of the foundation, the rate the tailings liquefy, the initial amount of liquefaction the tailings experience, as well as the presence of the excavation at the toe of the dam.

The softening characteristics of the foundation play a large role in allowing for the failure to occur, as without the progressive softening, the dam does not move without the liquefaction of tailings. Additionally, the reduced strength and rate at which the residual strength of the foundation plays a role, albeit relatively minor when compared to the presence of softening at all. Depth of the influence of the softening characteristics plays a relatively minor role in

final runout, as the failure is primarily a sliding failure.

The tailings influence the failure through two main mechanisms. Without liquefaction, the dam is not mobilized enough to travel the distances observed in the field. However, it was observed that liquefaction at certain distances from the dam no longer influenced the runout of the dam, as the dam stabilized before these material were able to mobilize, resulting primarily in the change of topography behind the dam. The rate of liquefaction has a direct influence on the runout, with more rapid liquefaction resulting in greater movements of the dam. On the other hand, the liquefied strength of the tailings does not have a significant impact on the runout behavior and distance of the final runout as long as the undrained shear strength is consistent with field observations.

The geometry of the failure, presented in the results by excluding the buttress stage 1 and omitting the excavation to prepare for the remaining buttress showed that without these changes, the runout was notably less. This is most likely the result of the excavation providing a voidspace for an additional area of dam to fill and continue moving through after the failure, and without the excavation, the downhill movements are reduced.

6.3 Future Work

Further improvements upon the model presented in this paper may be made, as well as applied to further simulations and models of other incidents and failures, either as a means of better understanding other post-failure kinematics, or a predictive effort for understanding risk.

- The addition of more advanced constitutive models for the tailings will be extremely valuable in providing additional, potentially more precise information on runout and

behavior for the tailings. The implementation of such models as NORSAND will be invaluable in improving understanding of liquefaction in the context of large deformation analyses, determining liquefaction extent and rate of liquefaction.

- Additionally, the tailings modeling could be improved too allow for the effect of unsaturated conditions and the increased strength as a result of suction, allowing for the examination of potential influence of the failure as the pore pressures and suction are relieved after the initial failure.
- For risk analysis on currently existing, unfailed dams, the application of material variability probability curves based on knowledge of the materials in the area can be used to construct multiple models to examine not only the potential for failure, but the consequences in the event of failure.

6.4 Closing Thoughts

MPM has been shown to be a valuable tool in understanding post-failure kinematics, as well as the effects associated with material variability. It provides valuable insight on influence of material behavior on runout and failure. In particular, the rate and quantity of liquefaction of the tailings as well as the strain-softening in the foundation play key roles in the failure of the Cadia Tailings Dam. The application of MPM shows the high potential of the method as a means of understanding risk, particularly with the recent developments contributing to the calls for increased regulation and safety with these structures.

Bibliography

- [1] M. Jefferies, N. Morgenstern, D. Van Zyl, and J. Wates, “Report on ntsf embankment failure, cadia valley operations, for ashurst australia,” 2019.
- [2] A. Yerro Colom, “Mpm modelling of landslides in brittle and unsaturated soils,” 2015.
- [3] L. N. Bowker and D. M. Chambers, “The risk, public liability, & economics of tailings storage facility failures,” *Earthwork Act*, pp. 1–56, 2015.
- [4] F. F. do Carmo, L. H. Y. Kamino, R. T. Junior, I. C. de Campos, F. F. do Carmo, G. Silvino, M. L. Mauro, N. U. A. Rodrigues, M. P. de Souza Miranda, C. E. F. Pinto, *et al.*, “Fundão tailings dam failures: the environment tragedy of the largest technological disaster of brazilian mining in global context,” *Perspectives in ecology and conservation*, vol. 15, no. 3, pp. 145–151, 2017.
- [5] “Global industry standard on tailings management,” *Global Tailings Review*, 2020.
- [6] N. Morgenstern, S. Vick, and D. Van Zyl, “Report on mount polley tailings storage facility breach: Independent expert engineering investigation and review panel,” *Retrieved from Mount Polley Review Panel website: <https://www.mountpolleyreviewpanel.ca/sites/default/files/report/ReportonMountPolleyTailingsStorageFacilityBreach.pdf>*, 2015.
- [7] M. Llano-Serna, D. J. Williams, and M. Ruest, “Analysis of tailings dam-break and run-out,” in *Tailings 2017, 4th International Seminar on Tailings Management, 12-14 July 2017, Santiago, Chile*, 2017.

- [8] B. Indraratna, L. Wijewardena, and A. Balasubramaniam, “Large-scale triaxial testing of grey wacke rockfill,” *Geotechnique*, vol. 43, no. 1, pp. 37–51, 1993.
- [9] R. Fell and G. Hunter, “The deformation behaviour of rockfill,” 2002.
- [10] G. Hunter, *The deformation behaviour of embankment dams and landslides in natural and constructed soil slopes*. PhD thesis, School of Civil and Environmental Engineering, University of New South Wales, 2003.
- [11] P. Robertson, “Evaluation of flow liquefaction: Influence of high stresses,” in *Proc., 3rd Int. Conf. on Performance Based Design (PBD-III), Vancouver: ISSMGE*, 2017.
- [12] A. Skempton, “First-time slides in over-consolidated clays,” *Geotechnique*, vol. 20, no. 3, pp. 320–324, 1970.
- [13] D. Sulsky, Z. Chen, and H. L. Schreyer, “A particle method for history-dependent materials,” *Computer methods in applied mechanics and engineering*, vol. 118, no. 1-2, pp. 179–196, 1994.
- [14] I. Jassim, D. Stolle, and P. Vermeer, “Two-phase dynamic analysis by material point method,” *International journal for numerical and analytical methods in geomechanics*, vol. 37, no. 15, pp. 2502–2522, 2013.
- [15] A. Yerro, E. Alonso, and N. Pinyol, “The material point method for unsaturated soils,” *Géotechnique*, vol. 65, no. 3, pp. 201–217, 2015.
- [16] L. Beuth, “Formulation and application of a quasi-static material point method,” 2012.
- [17] F. Ceccato, “Study of large deformation geomechanical problems with the material point method,” 2015.

- [18] L. E. Zambrano-Cruzatty, A. Yerro, and N. Stark, “Influence of the stiffness and saturated conditions of sand on the numerical simulation of free fall penetrometers,” in *Geo-Congress 2020: Modeling, Geomaterials, and Site Characterization*, pp. 9–18, American Society of Civil Engineers Reston, VA, 2020.
- [19] Z. Więckowski, S.-K. Youn, and J.-H. Yeon, “A particle-in-cell solution to the silo discharging problem,” *International journal for numerical methods in engineering*, vol. 45, no. 9, pp. 1203–1225, 1999.
- [20] C. Coetzee, A. Basson, and P. Vermeer, “Discrete and continuum modelling of excavator bucket filling,” *Journal of terramechanics*, vol. 44, no. 2, pp. 177–186, 2007.
- [21] P. Mackenzie-Helnwein, P. Arduino, W. Shin, J. Moore, and G. Miller, “Modeling strategies for multiphase drag interactions using the material point method,” *International journal for numerical methods in engineering*, vol. 83, no. 3, pp. 295–322, 2010.
- [22] P. Vermeer, L. Beuth, and T. Benz, “A quasi-static method for large deformation problems in geomechanics,” in *Proceedings of the 12th international conference of international association for computer methods and advances in geomechanics (IACMAG), Goa, India*, pp. 55–63, Citeseer, 2008.
- [23] Z. Więckowski, “The material point method in large strain engineering problems,” *Computer methods in applied mechanics and engineering*, vol. 193, no. 39-41, pp. 4417–4438, 2004.
- [24] I. K. a. Kafaji, *Formulation of a dynamic material point method (MPM) for geomechanical problems*. 2013.
- [25] C. M. Mast, *Modeling landslide-induced flow interactions with structures using the material point method*. PhD thesis, 2013.

- [26] K. Soga, E. Alonso, A. Yerro, K. Kumar, and S. Bandara, “Trends in large-deformation analysis of landslide mass movements with particular emphasis on the material point method,” *Géotechnique*, vol. 66, no. 3, pp. 248–273, 2016.
- [27] A. Yerro, K. Soga, and J. Bray, “Runout evaluation of oso landslide with the material point method,” *Canadian Geotechnical Journal*, vol. 56, no. 9, pp. 1304–1317, 2019.
- [28] F. Zabala and E. Alonso, “Progressive failure of aznalcóllar dam using the material point method,” *Géotechnique*, vol. 61, no. 9, pp. 795–808, 2011.
- [29] “Anura3d.” www.anura3d.com. Accessed: 2021-05-04.